TRAP GENERATION-ANNIHILATION AND CHARGING-DISCHARGING PROCESSES IN THIN OXIDES

By

SCOTT E. THOMPSON

A DISSERTATION PRESENTED TO THE GRADUATE SCHOOL
OF THE UNIVERSITY OF FLORIDA IN
PARTIAL FULFILLMENT OF THE REQUIREMENTS
FOR THE DEGREE OF DOCTOR OF PHILOSOPHY

UNIVERSITY OF FLORIDA

1992

UNIVERSITY OF FLORIDA LIBRARIES

ACKNOWLEDGEMENT

The author would like to thank Professors Chih-Tang Sah and Toshikazu Nishida for their time, support, and guidance throughout the course of this work. The participation on the qualifying examination and on the final defense by Professors F. A. Lindholm, A. Neugroschel, and K. A. Muttalib also merits a note of gratitude.

I am also grateful to Jack Kavalieros, Yi Lu, Michael Han, and Chetan Parikh for their friendship and assistance. The assistance from the highly professional staff of Janet Jones, Jenny Shannon, James Chamblee, and Jim Hales is appreciated. The financial support by an Intel Graduate Fellowship and Robert C. Pittman Eminent Scholar Chair Fellowship is gratefully acknowledged. Thanks are due to Dr. Leo Yau for support and being the mentor of the Intel Fellowship. Finally, I acknowledge my wife, Melanie Pecins-Thompson, for her persistent and continued support and encouragement.

TABLE OF CONTENTS

Page

ACKNOWLEDGEMENTS....ii

ABSTRACT....v

CHAPTERS

1 INTRODUCTION....1

2 DEVICE FABRICATION, EXPERIMENTAL SETUP, AND MEASUREMENT TECHNIQUES....6

2.1 Experimental Setup....6
2.2 Device Fabrication....11
2.3 Measurement Technique....14

3 A NEW MEASUREMENT METHOD FOR TRAP PROPERTIES IN INSULATORS AND SEMICONDUCTORS: USING ELECTRIC FIELD STIMULATED TRAP-TO-BAND TUNNELING TRANSITIONS IN SiO_2....19

3.1 Introduction....19
3.2 Experimental Method....24
3.3 Sample Preparation and Measurements....34
3.4 EFSE Applied to Thermal Oxides....39
3.5 Conclusion....73

4 TUNNELING AND THERMAL EMISSION OF ELECTRONS FROM A DISTRIBUTION OF SHALLOW TRAPS IN SiO_2....74

4.1 Introduction....74
4.2 Experimental Method....75
4.3 Temperature and oxide field dependence of oxide trap charging....76
4.4 Conclusions....85

5 POSITIVE CHARGE GENERATION IN SiO_2 BY ELECTRON-IMPACT-EMISSION OF TRAPPED ELECTRONS....87

5.1 Introduction....87
5.2 Experimental Method....93
5.3 Results....95
5.4 Conclusions....135

6 CONCLUSION....137

REFERENCES....139

BIOGRAPHICAL SKETCH....146

Abstract of Dissertation Presented to the Graduate School
of the University of Florida in Partial Fulfillment of the
Requirements for the Degree of Philosophy

TRAP GENERATION-ANNIHILATION AND CHARGING-DISCHARGING PROCESSES IN THIN OXIDES

By

Scott E. Thompson

May 1992

Chairman: Toshikazu Nishida
Cochairman: Chih-Tang Sah
Major Department: Electrical Engineering

New experimental data are presented which show that the initially neutral bridging oxygen vacancy (V_O), $[(Si\text{-}O)_3{\equiv}Si \cdot \; \cdot Si{\equiv}(O\text{-}Si)_3]$, is important in gate oxide charging. Two electron bound states for the defect are experimentally measured on industrial gate oxide, a shallow and deep level located 1eV and 7eV from the oxide conduction band. The shallow level is measured using a new experimental technique which we have developed for characterization of traps in insulators and semiconductors and have applied to SiO_2. The technique uses the electric field as the stimulant and the tunnel transition, the detrap-emission mechanism, to determine the

trap energy level. A distribution of shallow charged oxide traps in energy is found throughout 0-3eV below the oxide conduction band edge with a peak density of states between 0.9eV to 1.0eV. The measured shallow energy level at the peak density is consistent with the recent theoretical anticipation for a shallow state at a bridging oxygen vacancy. The measured deep level is concluded from electron generated positive oxide charge experiments. Experiments are presented which indicate for the first time that the positive charge located in the bulk oxide film probably results from creation of the E′ center, V_O^+ donor, due to emission of a trapped electron by electron impact at an initially neutral bridging oxygen vacancy, V_O. An impact electron threshold energy of 7eV is measured which is consistent with the theoretical calculated bound state energy of 7.8eV for a deep electron at the oxygen vacancy. Electron capture at the deep positive trap, $V_O^+ + e \rightarrow V_O$, is shown to limit the buildup of positive oxide charge during electron impact.

CHAPTER 1
INTRODUCTION

Since the first successful fabrication of the modern metal-oxide-semiconductor field effect transistor (MOSFET) using oxide thermally grown on a silicon substrate by Kahng and Attalla of Bell Laboratory in 1960[1], numerous researchers have investigated the instability of the drain current versus gate voltage (I_D-V_G) characteristics due to (i) charging-discharging and generation-annihilation of bulk oxide electron and hole traps and (ii) generation-annihilation of interface traps. Recently, Sah reviewed in detail the historical developments of the MOS transistor[2], the physical charging-discharging and generation-annihilation processes[3,4], and the experimental data on oxide and interface traps[5]. Sah[4] identified (i) eight trap generation-annihilation processes via hydrogenation, (ii) ten trap charging-discharging processes via elastic tunneling, and (iii) five trap charging-discharging processes via capture and emission. In this work, we present new experimental data on (i) trap-to-band tunneling emission of electrons from a distribution of shallow traps and (ii) electron-impact-emission of trapped electrons in SiO_2.

In Chapter 2, we outline the principles of the bipolar metal-oxide-semiconductor field-effect transistor (BiMOSFET) used in this work. The device operation that enables detailed study of the generation-annihilation

and charging-discharging processes is presented. The device fabrication, experimental setup, and measurement techniques are described.

In Chapter 3, electric field stimulated trap-to-band tunnel emission (EFSE), shown in Figure 1.1, is used in a new experimental technique for characterization of traps in insulators and semiconductors. Two EFSE techniques, the isochronal-EFSE and transient-EFSE, are described. Equations are developed which allow the trap energy levels to be calculated from experimental emission decay data. The (i) numerical error in calculating the energy level from the experimental data, (ii) sensitivity of the results on the effective mass and parabolicity of the dispersion relation in the energy gap, and (iii) the sensitivity of the results to the form of the tunneling transition rate are calculated. The techniques are applied to electron traps in thermally grown integrated-circuit grade SiO_2 to illustrate their accuracy and utility. An energy distribution of shallow charged oxide traps is found throughout 0-3eV below the oxide conduction band edge with a density of states peak at about 0.9 to 1.0eV. The centroid of the charged oxide traps is about 90A from the SiO_2/Si interface. The measured energy level at the peak density is consistent with recent theoretical calculations for the shallow state of a bridging oxygen vacancy, $[(Si\text{-}O)_3{\equiv}Si\cdot\ \cdot Si{\equiv}(O\text{-}Si)_3]$.

Chapter 4 applies the isochronal-EFSE technique to measure the oxide field and temperature dependence of the charging of existing oxide electron traps in SiO_2. At low oxide field, the experimental energy spectrum peaks at 0.9eV while the measured thermal activation energy for electron

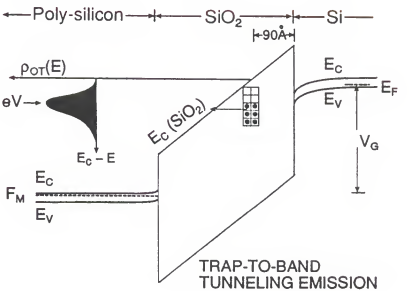

Fig. 1.1: Trap-to-band tunneling transition from shallow electron trap at the oxygen vacancy defect to the oxide conduction band.

detrapping is about 0.4eV. Their ratio, 0.9/0.4 = 2.25, is consistent with the Mott ratio of the Jahn-Teller effect for the polar SiO_2, 1.9.

In Chapter 5, experiments are presented which indicate for the first time that the positive charge located in the bulk oxide film probably results from creation of the E′ center, V_O^+ donor, due to emission of a trapped electron by electron impact at an initially neutral bridging oxygen vacancy V_O (Figure 1.2). To delineate the impact emission generation mechanism over other possible mechanisms, four sets of experiments are performed: (i) the kinetics of positive charge generation and neutralization of the positive traps by electron capture, (ii) the oxide current density, temperature, and gate oxide processing dependences of positive charge generation, (iii) the location of the positive charge through centroid measurements, and (iv) the electron threshold energy for positive charge generation.

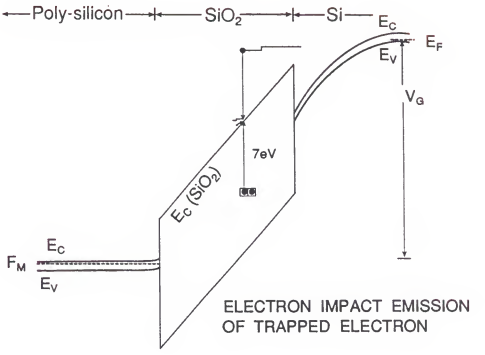

Fig. 1.2: Positive charge generation in SiO_2 by electron-impact-emission of an 7eV deep trapped electron at the oxygen vacancy defect.

CHAPTER 2
DEVICE FABRICATION, EXPERIMENTAL SETUP, AND MEASUREMENT TECHNIQUES

2.1 Experimental Setup

Figure 2.1 shows the cross-sectional view of the bipolar metal-oxide-semiconductor field-effect-transistor (BiMOSFET) and identifies the base, drain/collector, gate, source/collector, and emitter electrodes. Figure 2.2 illustrates the biasing of the device during substrate electron injection. In our substrate electron injection stress experiments, the vertical npn transistor is used to inject hot electrons into the gate oxide. As indicated in Figure 2.2, an inversion layer is induced by the gate voltage, V_{OX}, applied between the gate and the source/collector and drain/collector electrodes which are connected together. The (n+/n-) substrate to p-well emitter/base junction is forward biased (V_{EB}) to inject the electrons into the Si surface space-charge layer beneath the n-type surface inversion layer formed under the gate oxide of the MOSFET. The reverse bias (V_{CB}), applied to the n+collector/p-well collector/base junction (same as the n+ source and n+ drain/p-well junctions), forms a surface space-charge-layer beneath the gate inversion layer. Thus, the injected electrons from the emitter are accelerated by the electric field in the Si surface space-charge layer towards the SiO_2/Si interface. Those electrons that have gained a kinetic energy

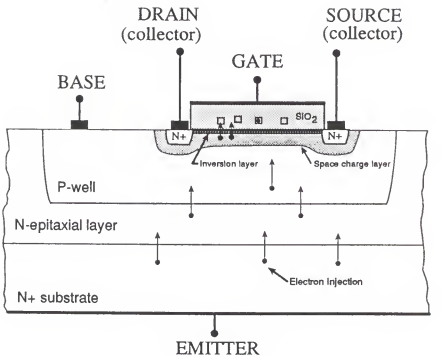

Fig. 2.1: Cross-sectional view of the bipolar metal-oxide-semiconductor field-effect transistor.

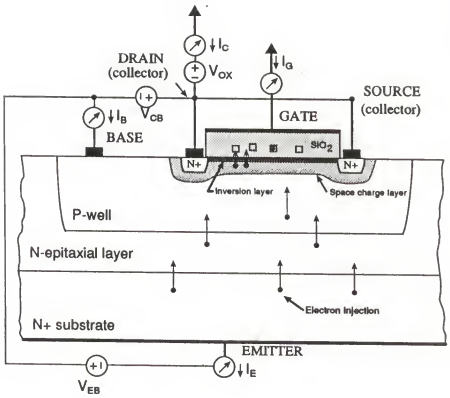

Fig. 2.2: Electrode labels and biasing of the bipolar metal-oxide-semiconductor field-effect transistor during substrate electron injection.

greater than the SiO_2/Si barrier energy (=3.02eV) are injected into the oxide. Before exiting the oxide into the poly-Si gate, these injected electrons may (1) be trapped by an existing (as-grown or native) or newly generated oxide electron trap, charging the existing trap negatively, or (2) be accelerated by the oxide electric field and after gaining enough kinetic energy (i) release a trapped electron by impact collision, charging the existing trap positively, (ii) generate a new oxide electron trap by breaking a strained intrinsic bond (Si:Si or Si:O), a hydrogen bond (Si:H, SiO:H, SiCl:H, SiOCl:H and others), or an impurity bond (Si:Cl, SiO:Cl, and silicon and oxygen bonded with halogen, carbon, or other impurities) in the oxide, (iii) generate a plasmon or hole near the gate conductor/oxide interface, or (iv) release H from the gate conductor.

The unique feature of the substrate injector structure is that the oxide electric field can be controlled independently from the gate electron current density. Thus, the electric field dependences of the charging-discharging and generation-annihilation rates for oxide and interface traps can be measured under experimental conditions where one mechanism is dominant. This allows their individual contributions to the threshold voltage shift to be extracted. The density of each trap species can also be determined.

During each oxide stressing experiment, the average oxide electric field is held constant by applying a constant DC voltage, $V_{GD}=V_G-V_D=V_{GS}=V_G-V_S$=constant, between the gate electrode (V_G) and inversion layer ($V_D=V_S$). The gate current (I_G) is also kept constant during the stress by controlling the forward bias emitter voltage of the BJT (V_{EB}) using

current meters and power supplies controlled by digital feedback on a MicroVAX-II via a IEEE-488 bus. Figure 2.3 shows a schematic diagram of the experimental setup. The degradation is monitored by periodically interrupting the stress and measuring (i) the drain current versus gate voltage (I_D-V_G) and (ii) the gate capacitance versus gate voltage (C_G-V_G) curves. The device temperature is maintained constant during each measurement run using the MicroVAX-II, IEEE-488 bus, and a liquid nitrogen dewar system. The temperature controller was developed by Sah and his graduate students over many years[6].

2.2 Device Fabrication

The gate oxides are grown on two types of (100) Si wafers: (i) boron-implanted p-well on a n^-/n^+ substrate and (ii) p-epitaxial layer on a n^+ substrate. The p-well is 2.8μm in depth and has a surface boron concentration of $2x10^{16}cm^{-2}$. The p-epitaxial layer is 13μm thick and has a uniform doping of $3x10^{16}cm^{-2}$. Three industrial oxidation processes are used: 850C dry/wet/dry, 900C dry, and 950C partial steam. The dry oxide is grown with 0.0% and 0.3% trichloroethane in the oxidation ambient. The gate oxide thickness covers the range of 86 to 281A. Immediately following the gate oxidation growth, a 3500 or 5500A thick poly-crystalline silicon gate is deposited and doped n-type by $POCl_3$. The oxidized wafers with the poly-silicon layer are then processed to fabricate the self-aligned n^+ poly-silicon gate BiMOSFET test structure. Figures 2.4 and 2.5 show a flow chart of the device fabrication schedule. Next, the self-aligned source and

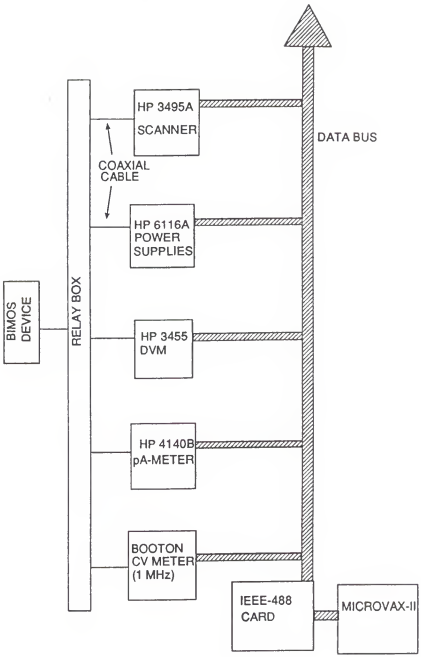

Fig 2.3: Schematic diagram of the substrate injection experimental setup designed for gate oxide electron injection stress, C_G-V_G, and I_D-V_D measurements.

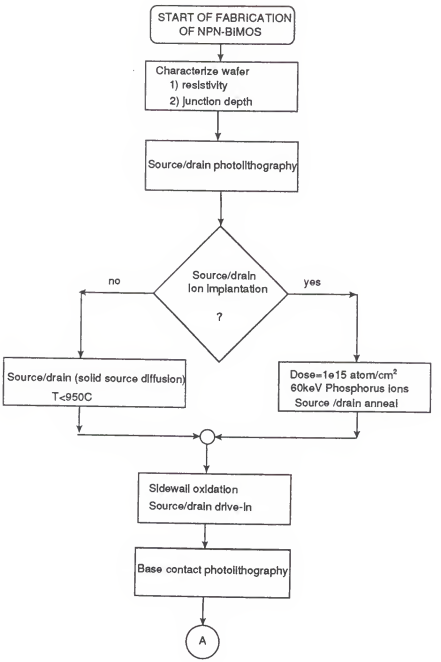

Fig 2.4: Flow chart for the substrate injector test structure fabrication process.

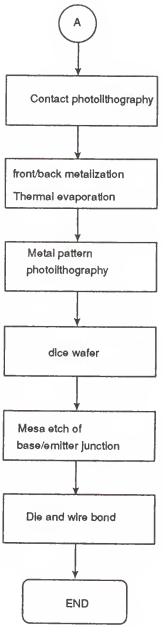

Fig 2.5: Flow chart for the substrate injector test structure fabrication process.

drain junctions are implanted with 1.0 x $10^{15}cm^{-2}$ of 60KeV phosphorus ions. The source and drain implantation damage was annealed at 850C for 30 minutes in N_2. The source and drain are then diffused at 800-1000C for 2 hours in a nitrogen or oxygen ambient. Variations in the diffusion temperature are done in order to introduce oxide defects intentionally. High purity VLSI-MOS grade aluminum is then thermally evaporated and patterned to form the ohmic contacts. No passivation is deposited on the wafers. Linear and reentrant geometries of many gate areas are measured giving similar results. The reproducibility of results is good with device to device variations in the gate voltage shift typically much less than 10%.

2.3 Measurement Technique

2.3-1 Bulk Oxide Charge

During electron injection into the gate oxide at 77-294K and low oxide fields (less than 3.0MV/cm), only existing (as-fabricated) oxide traps capture electrons and become negatively charged. Generation of new oxide electron traps is minimized by limiting the electron injection to this low field range. The electron injection is periodically stopped to measure the gate capacitance versus gate voltage (C_G-V_G) and drain current versus gate voltage (I_D-V_G) curves at 77K. Parallel positive gate voltage shift of the C_G-V_G and I_D-V_G curves is observed which indicates charging of existing oxide electron traps and not the generation of new interface traps. The C_G-V_G and I_D-V_G curves are shown in Figures 2.6 and 2.7. The identical gate voltage shift of the I_D-V_G and C_G-V_G curves indicates areally uniform

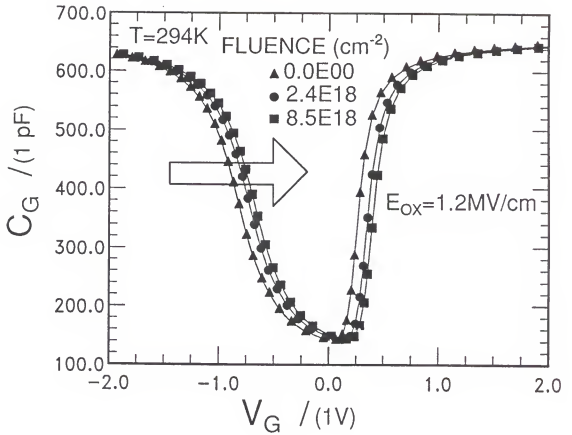

Fig. 2.6: Gate capacitance versus gate voltage after an electron fluence and E_{OX}=1.2MV/cm at T=294K.

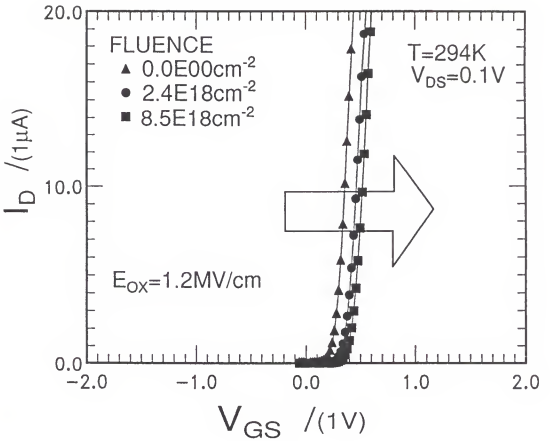

Fig. 2.7: Drain current versus gate voltage after an electron fluence and E_{OX}=1.2MV/cm at T=294K.

charging of oxide traps because the I_D-V_G curve is sensitive to oxide charge localized near the source while the C_G-V_G curve is sensitive to oxide charge along the entire surface channel. The gate voltage applied during the measurement of the C_G-V_G and I_D-V_G curves is always much lower than the gate voltage applied during electron injection so that electrons are not detrapped via trap-to-band tunneling transitions during the C_G-V_G and I_D-V_G measurements.

The number of charged oxide traps, $n_{OT}(\#/cm^2)$, is obtained from the gate voltage shift using

$$n_{OT}(X_{OT},t) = (1/qX_{OT}) \int_0^{X_{OX}} x\rho_{OT}(x,t)\,dx$$

$$= (\varepsilon_{OX}/q)(\Delta V_G/X_{OT}) \qquad (2.1)$$

where ρ_{OT} is the oxide charge density per unit volume$(\#/cm^3)$, X_{OX} is the oxide thickness, X_{OT} is the centroid of the oxide charge measured from the gate-conductor/oxide interface, ε_{OX} is the static permitivity of SiO_2, and q is the magnitude of the electronic charge. In the calculation of the density of native oxide traps, N_{OT}, we either (1) measure the centroid of the charge or (2) equate the centroid to the oxide thickness. If the centroid is equated to the oxide thickness, i.e. X_{OT}=X_{OX} is assumed, this gives the effective oxide trap density located at the SiO_2/Si interface which would give the same amount of Si energy band bending as the distributed oxide traps. This has been used universally as a characterization parameter of oxide trap since

the centroid and the thickness variation of the oxide trap (volume) density has proved to be very difficult to measure accurately especially in thin oxides (by step etch in thick oxides). In Chapters 3 and 5, measurements for the oxide trap centroid are presented along with the limitations of the techniques.

2.3-2 Interface Trap

The interface trap generation is measured after electron injection into the oxide at room temperature and oxide fields between 1 and 7MV/cm. The electron injection is periodically stopped to measure the C_G-V_G and I_D-V_G curves at the stress temperature. From the distortion in the C_G-V_G, the change in the number interface states between flatband (V_S=0) and inversion (V_S=2Φ_F) is calculated using

$$N_S = \varepsilon_o (\Delta V_{INV} - \Delta V_{FB}) / (qX_{OX}) \qquad (2.2)$$

where ΔV_{INV} and ΔV_{FB} are the gate voltage shifts of the inversion and flatband capacitances.

CHAPTER 3
A NEW MEASUREMENT METHOD FOR TRAP PROPERTIES IN INSULATORS AND SEMICONDUCTORS - USING ELECTRIC FIELD STIMULATED TRAP-TO-BAND TUNNELING TRANSITIONS IN SiO_2

3.1 Introduction

In Chapter 3, a new experimental technique for characterization of traps in insulators and semiconductors and its speed-up derivative are presented which use trap-to-band tunneling emission of electrons. Equations are given which allow the energy levels to be calculated from experimental emission decay data. The expressions are valid for electrically active defects with a discrete energy level or a distribution of levels. The numerical error in calculating the energy level from experimental data is 1-2% for a given set of energy-band parameters such as the effective masses and the parabolicity of the dispersion relation in the energy gap. The techniques are applied to electron traps in thermally grown integrated-circuit grade SiO_2 to illustrate their accuracy and utility. An energy distribution of shallow charged oxide traps is found throughout about 0-3eV below the oxide conduction band edge with a peak density of states at about 0.9 to 1.0eV. The centroid of the charged oxide traps is about 82A from the SiO_2/Si interface. The same density-energy curve is observed for oxide traps in many thermally grown dry oxide films thicker than 150A. A

decrease in the density of the charged oxide traps is found for oxides less than 100A. A distribution of capture cross sections versus trap energy depth, ranging from 10^{-15} to $10^{-17}cm^2$, is measured at low oxide electric field (1.1 MV/cm). The shallower traps have a larger capture cross section than the deeper traps. The measured energy level at the peak density is consistent with the recent theoretical anticipation for an oxygen vacancy which relaxes to form a silicon-silicon bond in the oxide, $[(Si\text{-}O)_3{\equiv}Si \cdot \cdot Si{\equiv}(O\text{-}Si)_3]$.

Previously, electron traps due to intrinsic and extrinsic defects in semiconductors and insulators have been widely studied using thermally stimulated conductivity (TSC) and luminescence (TSL) [7], thermally stimulated capacitance (TSCAP) [8], and voltage stimulated capacitance (VSCAP) first developed by Yau and Sah in 1971 [9] later known as DLTS (deep level transient spectroscopy) and CTS (capacitance transient spectroscopy). In these techniques, the thermal detrap-emission rate of the bound electrons making quantum mechanical transition to the conduction band is measured as a function of temperature to give the thermal activation energy of the detrap-emission transition mechanisms. Optical binding energy can be similarly obtained using optical stimulation by varying the photon energy such as the optically stimulated capacitance transient (OSCAP) first reported by Sah, Rosier, and Forbes in 1969 [10] or the corresponding optically stimulated current (OSC) transient first reported by Sah and Tasch in 1967 [11].

In this chapter, a new variation of these methods is demonstrated by us in which the electric field is the stimulant and tunnel transition, the

detrap-emission mechanism, which is to be abbreviated as transient and isochronal-EFSE which stands for electric-field stimulated tunnel emission spectroscopy. As illustrated in Fig. 3.1, the oxide electric field is employed to stimulate trap-to-band detrap-emission transitions. The use of EFSE offers several advantages over TSC, TSL, TSCAP, VSCAP (DLTS or CTS), and OSCAP and OSC: (1) the electric field is somewhat easier to control and vary in a prescribed manner with time than the temperature and much easier to vary than photon energy; and (2) EFSE measures the trap-to-band transition via tunneling which has little or no lattice relaxation (Franck-Condon transition) just like the optically simulated emission (OSCAP and OSC) while the thermally stimulated transition is between equilibrium states of the system of lattice vibrations and electrons which could involve large lattice relaxation. Hence, the tunnel transition energy measured by EFSE, like the optical transition energy measured by OSCAP and OSC, is equal to the energy level of the trapped electron, while the thermal activation energy measured by TSC, TSL, TSCAP, DLTS and the other thermally stimulated emissions is smaller than the energy level if the lattice relaxes significantly in the vicinity of a trap after an electron is detrapped-emitted or trapped-captured by the trap.

Although vast experimental data on trap energy level or thermal activation energy in semiconductors (Si, GaAs, etc.) have been reported using the thermally stimulated techniques, few experimental energy level data have been reported on the shallow and deep electron and hole bound states in amorphous insulating materials [12,13]. Most of the recent work

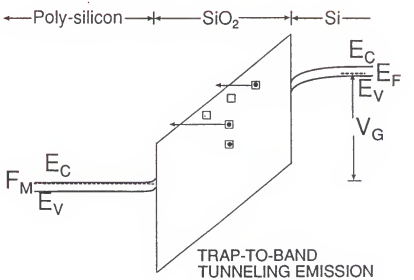

Fig. 3.1: Electric field stimulated trap-to-band tunneling transition in SiO_2.

on electron trapping on integrated circuit grade amorphous SiO_2 films has been limited on the magnitude of the electron and hole capture cross section and trap density. Recent literature reviews on traps in oxide film grown on integrated circuit grade crystalline silicon were given by Sah and Hsu [14] and Young [15]. Energy levels for intrinsic traps in SiO_2 have been also speculated and estimated theoretically [13-19].

In the next chapter (Chapter 4) we use the new isochronal-EFSE technique on SiO_2 to measure an energy distribution of traps charged under various temperatures and oxide electric fields[12]. The distribution has a peak located about 0.9 to 1.0eV below the oxide conduction band edge and a thermal activation of 0.4eV. The large difference in tunnel and thermal activation energy suggests that lattice relaxation (Jahn-Teller effect) is perhaps very strong. We note that the ratio of tunneling-to-thermal activation energy, 0.9/0.4=2.2, is fairly consistent with the Mott-Gurney ratio [20] of static-to-optical dielectric constant of SiO_2, 3.9/2.1=1.9. In view of these encouraging results, we would like to present detailed analyses of the EFSE methods to provide guides for future applications of the methods. These include the following: (i) A detailed analysis is given of the original transient-EFSE technique from which the isochronal-EFSE is derived. (ii) The isochronal-EFSE is assessed and compared with the original and more exact transient-EFSE technique. (iii) The two techniques are illustrated by numerical calculations of a Gaussian distribution of electron traps. And (iv) the two techniques are experimentally compared on the evaluation of the energy levels of electron traps using experimental data taken on thermally grown SiO_2.

3.2 Experimental Method

The EFSE techniques are similar to the TSC, TSCAP, VSCAP (DLTS) and other stimulated detrap-emission techniques in which electron (or hole) traps are first populated with electrons (or holes). In the thermally stimulated detrap-emission techniques, the temperature is then increased to measure the change of the number of trapped electrons Δn_T over a range of temperature, ΔT. A peak in $\Delta n_T/\Delta T$ gives the thermal activation energy for electron detrap-emission. The monitored parameter to give Δn_T is either a change in current (TSC) or capacitance (TSCAP and VSCAP-DLTS) due to the application of the stimulant (temperature change or voltage change). Electrons bound at traps with larger activation energies are detrapped-emitted at higher temperatures since thermal detrapping rate increases exponentially with temperature.

In EFSE measurements, after the electron traps are populated, the electric field is incrementally increased. At low electric field, electrons at shallower traps are detrapped-emitted by trap-to-band tunnel transitions. As the electric field increases, electrons from increasingly deeper traps are detrapped-emitted via tunneling. The differential change in the number of trapped electrons with respect to the change in the electric field, $\Delta n_T/\Delta E_{OX}$, is monitored. The quantity of $\Delta n_T/\Delta E_{OX}$ in EFSE is analogous to $\Delta n_T/\Delta T$ in the thermally stimulated methods. In the following sections, a closed form expression between $\Delta n_T/\Delta E_{OX}$ and the areal density of charged oxide traps, $D_{OT}(\#/eV\text{-}cm^2)$, is obtained.

3.2-1 Transient-EFSE Technique

The transient-EFSE technique consists of the following four steps: (1) the electron traps are charged via capturing injected electrons for a time t_c at 77K and at a low constant oxide electric field using the bipolar metal-oxide-semiconductor transistor (BiMOS) [21] test structure; (2) the electron injection into the oxide is stopped; (3) a constant oxide electric field, E_{OX} (the discharge-detrap-emission field), is applied to stimulate tunnel emission of trapped electrons from the oxide traps to the oxide conduction band through a triangular potential barrier; and (4) the trapped electron density versus detrap-emission time, t_e, is measured.

To monitor (1) and (4), the charging or discharging field is interrupted and the gate voltage shift, ΔV_G, versus charging-capture, t_c, or discharging-detrap-emission time, t_e, is measured from the MOSFET drain current-gate voltage (I_D-V_G) and gate capacitance-gate voltage (C_G-V_G) curves. This is repeated at a succession of discrete discharging-detrap-emission times to give many I_D-V_G and C_G-V_G curves, one from each detrap-emission time. To determine the density-of-state, the ΔV_G-t_e curve is repeated at many discharging-detrap-emission oxide electric fields.

The number of charged oxide traps, n_{OT}(#/cm^2), is obtained from the gate voltage shift using

$$n_{OT}(X_{OT},t) = (1/qX_{OT}) \int_0^{X_{OX}} x\rho_{OT}(x,t)\,dx = (\varepsilon_{OX}/q)(\Delta V_G/X_{OT}) \quad (3.1)$$

where ρ_{OT} is the volume oxide charge density (#/cm^3), X_{OX} is the oxide thickness, X_{OT} is the centroid of the oxide charge measured from the gate-conductor/oxide interface, ε_{OX} is the static permitivity of SiO_2, and q is the magnitude of the electronic charge. $t=t_c$ for (1) and $t=t_e$ for (4).

After the electron traps are charged by electron capture at 77K in a low oxide electric field in step (1), the electron injection is stopped at time $t=0^-$ in step (2). At time $t=0^+$ in step (3), a constant oxide electric field is applied to stimulate tunnel emission of the trapped electrons. The number of oxide traps that remain charged or the number of electrons that remain trapped remain charged after a tunnel emission time t_e at a discharge-detrap-emission oxide field E_{OX} is

$$n_{OT}(t_e) = \int_{E_V}^{E_C} \exp(-\omega t_e) D_{OT}(E_T)\, dE_T \qquad (3.2)$$

where D_{OT} (#/eV$\cdot$cm^2) is the initial density of charged oxide traps. The trap-to-band tunneling transition rate, ω, from the Price-Sah model[22] is

$$\omega = (\pi^2/h^3)(m_y m_z)^{1/2}(E_{OX}/E_T)W^2 \exp(-2\Theta) \qquad (3.3)$$

$$\Theta = (4\pi/3)(2m_x)^{1/2} E_T^{3/2}/(hE_{OX})\,. \qquad (3.4)$$

The energy level of the oxide electron trap, E_T, is measured from the oxide conduction band edge. W^2 is the square of the tunneling transition matrix element. The new transient-EFSE technique measures $n_{OT}(t_e)$ from the gate-voltage shift versus time while a constant DC electric field is applied across the oxide. Many $n_{OTi}(t_e)$ vs t_e curves are measured, one from each

discharge oxide electric field, E_{OXi}. The term, $\exp(-\omega t_e)$, in Eq. (3.2) gives the probability that a trapped electron at a energy E_T has not made a trap-to-band tunneling transition after a detrap-emission time t_e. ω_i is the tunneling rate at the i-th applied oxide electric field (E_{OXi}). Figure 3.2 plots $\exp(-\omega_i t_e)$ versus electron trap energy at a fixed detrap-emission time (t_e) for two oxide fields. Traps located in energy within the shaded region are emitted at E_{OXi+1} but not E_{OXi}. Since $\exp(-\omega_i t_e)$ is a double exponential function in E_T, the function can be approximated as a unit step function in energy. Thus, the experimental data, $\partial n_{OT}/\partial E_{OX} = [n_{OTi+1}(t_e)-n_{OTi}(t_e)]/(E_{OXi+1}-E_{OXi})$, are proportional to the density of states of the charged oxide traps between the energy range $(E_{Ti+1}-E_{Ti})$, as seen in Fig. 3.2. E_{Ti} is obtained from $(\partial^2/\partial E_T^2)[\exp(-\omega_i t_e)] = 0$ and given accurately by $\omega_i t_e = n$, where n=1. The error in E_{Ti} is only 0.69% if n=1 is used as compared to the exact solution at n=1.45 obtained by solving $(\partial^2/\partial E_T^2)[\exp(-\omega_i t_e)] = 0$ through iteration. The density of states is then computed from

$$D_{OT}(E_{Ti}) = [n_{OTi}(t_e) - n_{OTi+1}(t_e)] \; / \; [E_{Ti+1} - E_{Ti}] \qquad (3.5)$$

$$= (C_O/q)\,(X_{OX}/X_{OT})\,[\Delta V_{Gi}(t_e) - \Delta V_{Gi+1}(t_e)] / [E_{Ti+1} - E_{Ti}] \qquad (3.6)$$

Equation (3.6) is valid for traps at a discrete energy level or a distribution of traps because of the very large energy dependence from the double exponential $\exp(-\omega t_e)$ in which ω is also an exponential in energy E_T given by Eq. (3.3).

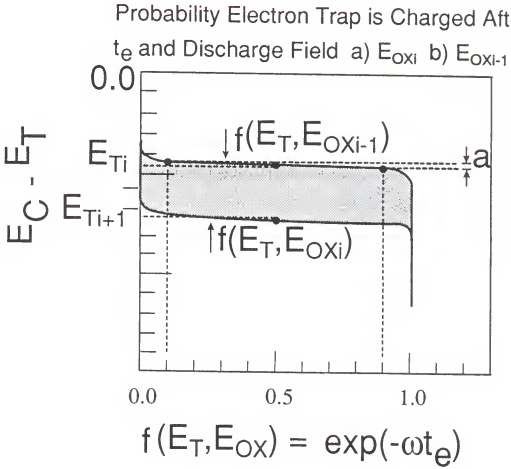

Fig. 3.2: Tunneling probability, $\exp(-\omega_i t_e)$, for two values of oxide field at time t_e. Electrons bound in energy within the shaded region undergo trap-to-band transitions at E_{OXi} but not at E_{OXi-1}.

The accuracy of the technique including the effect of using different detrap-emission time is now calculated. Consider a density of states for the charged oxide traps given by the Gaussian distribution $D_{OT}=Aexp[-(E_T-0.9eV)^2/C]$ where $C=0.1(eV)^2$ and $A=3.0x10^{12}eV^{-1}cm^{-2}$. Initially, the number of charged traps, $n_{OT}(t_e=0^- \text{ sec.})$, is equal to the integral of D_{OT} over energy as indicated by $t_e=0$ in Eq. (3.2). Equation (3.2) is used to calculate the number of charged oxide traps versus time at a constant discharge oxide field, $n_{OT}(t)$, for discharge fields between 0.1 and 5.0 MV/cm in 0.05MV/cm increments. Ten of the $n_{OT}(t)$ versus time curves are shown in Fig. 3.3. From the family of curves at different discharge fields, $[n_{OTi}(t_e)-n_{OTi+1}(t_e)]/(E_{OXi+1}-E_{OXi})=-\partial n_{OT}/\partial E_{OX}>0$ versus the oxide field are calculated at the discharge-emission times of $t_e=5.0$, 50.0, 500.0, and 1000.0 seconds and shown in Fig. 3.4. Equation (3.5) is then used to calculate the density of the initially charged traps as a function of trap energy level. The calculated spectrum is compared to the assumed Gaussian density of states in Fig. 3.5. Excellent agreement is obtained for the discharge-emission times between 5.0 and 1000.0 seconds. The calculated location of the peak in the density of states differs less than 1.0% from the assumed value of 0.9eV.

3.2-2 Isochronal-EFSE Technique

In this section, the accuracy of the much faster isochronal-EFSE technique[12] is evaluated by comparison with the exact transient-EFSE technique just described. The density of state can be obtained from the isochronal-EFSE technique in one measurement run while the exact transient-EFSE technique requires many measurements on one device.

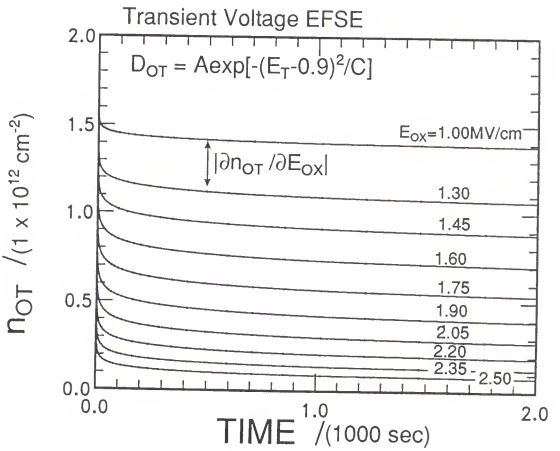

Fig. 3.3: Numerical calculation for the voltage transient-EFSE technique. Number of charged traps versus time for 10 values of the discharge field. To evaluate the tunneling transition rate, $W^2=10^{-24}V^2cm^3$ and $m_x=m_y=m_z=m_o$ were used.

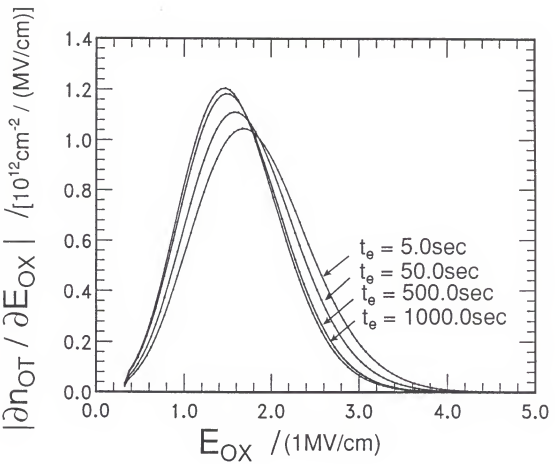

Fig. 3.4: $|\partial n_{OT}/\partial E_{OX}|$ evaluated at t_e equal 5.0, 50.0, 500.0, 1000.0 sec.

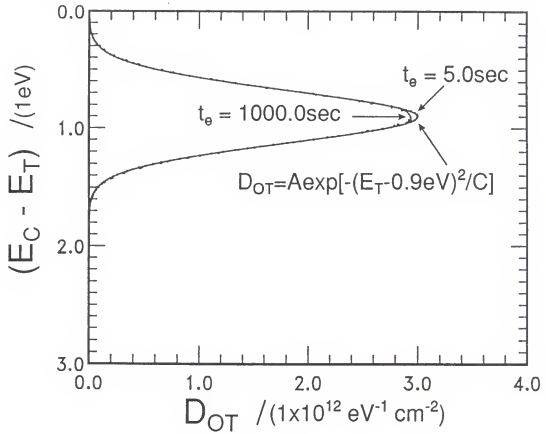

Fig. 3.5: Calculated density of traps compared to known density.

Thus, the isochronal-EFSE is much faster. It is nearly as accurate as the exact transient-EFSE because of the double exponential as we shall next show. The isochronal-EFSE technique consists of the following steps: (1) the oxide electron traps are first charged at 77K and a low constant oxide electric field by electron injection into the oxide using the BiMOS structure; (2) the electron injection is stopped; (3) the oxide electric field (discharge field) is increased in increments (typically 0.1MV/cm each) and maintained constant for the same isochronal time t_e at each field increment; and (4) at the end of detrap-emission for a time t_e, the gate voltage shift is measured to record the progress of electron detrapping via tunnel-emission transitions from the oxide traps.

The number of charged oxide traps after the i-th field increment is

$$n_{OTi}(E_{OXi}) = \int_{E_V}^{E_C} D_{OT}(E_T)\,[\exp(-\omega_i t_e)\cdot \exp(-\omega_{i-1} t_e)\ldots\exp(-\omega_1 t_e)]\,dE_T. \qquad (3.7)$$

If $\exp(-\omega_1 t_e)$ is approximated by a step function, then the density of states can be approximated by

$$D_{OT}(E_{Ti}) = [n_{OTi}(E_{OXi}) - n_{OTi+1}(E_{OXi+1})]/[E_{Ti+1} - E_{Ti}] \qquad (3.8)$$

$$= (C_O/q)(X_{OX}/X_{OT})[\Delta V_{Gi+1}(E_{OXi+1}) - \Delta V_{Gi}(E_{OXi})]/[E_{Ti+1} - E_{Ti}] \qquad (3.9)$$

which are similar but not identical to the exact Eqs. (3.5) and (3.6). The accuracy of Eqs. (3.8) and (3.9) compared with the exact Eq. (3.6) is now shown by a numerical calculation. The same Gaussian density of states expression used to calculate the accuracy of the transient-EFSE for Eqs. (3.5) and (3.6) is chosen. Electron detrapping via tunnel transitions is calculated as the oxide field is increased in 0.1MV/cm increments and maintained constant for a detrap-emission time t_e. Equation (3.3) is used to evaluate the tunnel transition rate. Equation (3.7) is used to calculate the number of traps which remain charged at t_e after each oxide electric field increment. n_{OT} versus discharge-detrap or tunnel-emission electric field curves are shown in Fig. 3.6. Four choices of isochronal discharge times are used, 5.0, 50.0, 500.0, and 1000.0 seconds to assess its effect. $|\partial n_{OT}/\partial E_{OX}|$ is calculated and shown in Fig. 3.7. The four spectra of initially charged traps calculated using Eq. (3.8) at the four assumed isochronal discharge-emission times is compared to the assumed spectrum in Fig. 3.8. The results of Fig. 3.8 show that the numerical error caused by the isochronal approximation is less than 2.0% in the density of states peak when using an isochronal detrap-emission time between 5.0 to 1000.0 sec.

3.3 Sample Preparation and Measurements

3.3-1 Sample Preparation

Details of the experimental setup and BiMOS test structure were described previously [12,21,23]. The gate oxides were grown on two types of (100) Si wafers: (i) boron-implanted p-well on a n^-/n^+ substrate and

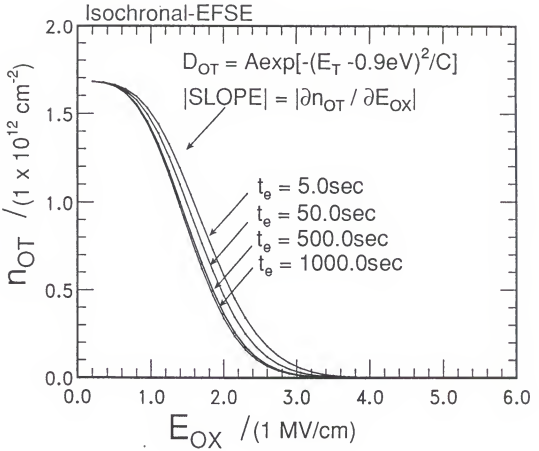

Fig. 3.6: Numerical calculation for the isochronal-EFSE technique. Number of charged traps after each t_e step versus discharge-emission field which is increased in 0.1MV/cm increments and maintained constant for t_e equal 5.0, 50.0, 500.0, and 1000.0 sec.

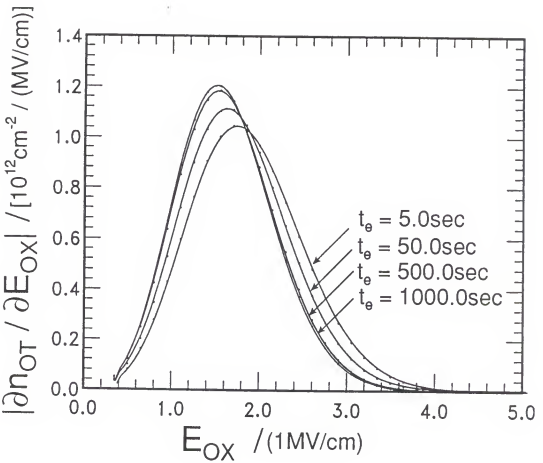

Fig. 3.7: $|\partial n_{OT}/\partial E_{OX}|$ evaluated at t_e equal 5.0, 50.0, 500.0, 1000.0 sec.

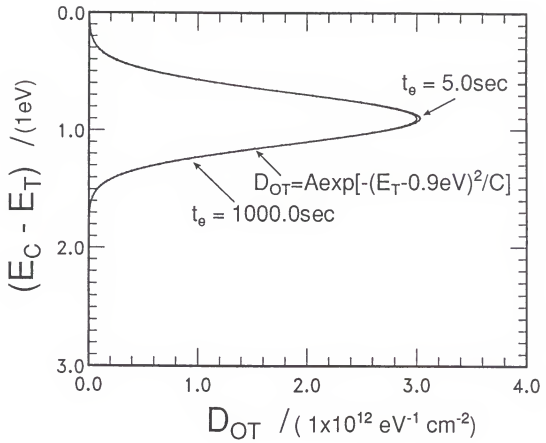

Fig. 3.8: Calculated density of traps compared to assumed density.

(ii) p-epitaxial layer on a n^+ substrate. Three oxidation processes were used: 850C dry/wet/dry, 900C dry, and 950C partial steam. The gate oxide thickness covered the range of 86 to 281A. Immediately following the gate oxidation growth, a 3500 or 5500A thick poly-crystalline silicon gate is deposited and doped n-type by $POCl_3$. The self-aligned source and drain junctions were implanted with $1.0 \times 10^{15} cm^{-2}$ of 60KeV phosphorus ions. The source and drain implantation damage was annealed at 850C for 30 minutes. The source and drain were then diffused at 950C for 90 minutes in a nitrogen ambient. High purity VLSI-MOS grade aluminum was then thermally evaporated and patterned to form the ohmic contacts. No passivation was deposited on the wafers. Linear and reentrant geometries of many gate areas were measured giving similar EFSE results.

3.3-2 Trap Charging by Electron Capture

Electrons are injected into the gate oxide at 77K and low oxide fields (0.5 to 1.0MV/cm) to charge existing (as-fabricated) oxide traps. Generation of new oxide electron traps is minimized by limiting the electron injection to this low field range[12,23,24]. The electron injection is periodically stopped to measure the gate capacitance versus gate voltage (C_G-V_G) and drain current versus gate voltage (I_D-V_G) curves at 77K. Parallel positive gate voltage shift of the C_G-V_G and I_D-V_G curves is observed which indicates charging of existing oxide electron traps and not the generation of new interface traps. The identical gate voltage shift of the I_D-V_G and C_G-V_G curves indicates areally uniform charging of oxide traps because the I_D-V_G curve is sensitive to oxide charge localized near the source while the C_G-V_G curve is sensitive to oxide charge along the entire surface channel. The gate

voltage applied during the measurement of C_G-V_G and I_D-V_G curves is always much lower than the gate voltage applied during electron injection so that electrons are not detrapped via tunneling during the C_G-V_G and I_D-V_G measurements.

3.4 EFSE Applied to Thermally Grown Oxides

In this section, the transient- and isochronal-EFSE techniques are used to measure electron traps in SiO_2. This section contains the results on: (1) the EFSE techniques applied to SiO_2; (2) the centroid for the oxide charge; (3) the reversibility of the charging and discharging process; (4) the measured capture cross section (σ_n^t) as a function of trap energy; and (5) the sensitivity of the measured energy spectrum on assumed Price-Sah model parameters.

3.4-1 Transient-EFSE Applied to Integrated-Circuit Grade Oxides

The transient-EFSE technique is applied to many BiMOS test devices with 184A thick VLSI (very large scale integrated) circuit grade oxides grown in a dry/wet/dry (850C) ambient. Electron traps are initially charged at 77K, 0.54MV/cm oxide field, oxide current density J_{OX}=0.26μA/cm^2, and charging time of 5.55x10^2 seconds to give an injected fluence of N_{INJ}=9.0x10^{14}/cm^2. Only a fraction of the initially neutral traps captures an electron and become negatively charged at this injected fluence. Thus, the oxide electric field is given accurately by (V_{OX}/X_{OX}) and not altered by the oxide charge as will be shown in section 3.4-5. Next, a constant oxide field is applied at 77K, and the gate voltage shift versus time is measured to

monitor the electron detrapping. The above procedure is repeated for twenty discharge fields ranging from 0.54 to 4.0MV/cm. Figure 3.9 shows the measured gate voltage shift versus time, $\Delta V_G(t)$, for ten of the discharge fields. The shift is defined with respect to the unstressed device. Figure 3.10 shows $|\partial n_{OT}/\partial E_{OX}|$ versus oxide electric field evaluated at t_e equal to 15.0, 50.0, and 500.0 seconds. The centroid for the oxide charge is assumed to be located at the SiO_2/Si interface, i.e. $X_{OT}=X_{OX}$ in Eq. (3.6). This assumption will be corrected in section 3.4-3. The density of states is calculated using Eq. (3.5) and plotted in Fig. 3.11. To evaluate the tunneling transition rate, $W^2=10^{-24}V^2cm^3$ and $m_x=m_y=m_z=m_o$ were used. The sensitivity of the density of states to the values of these parameters is discussed in section 3.4-7. A peak between 0.9-1.0eV in the experimental density of state is observed in the many BiMOS test devices. There is approximately 5% device-to-device variation in the measured density of traps. A point on the spectrum is calculated by subtracting two curves in Fig. 3.9 which come from two different devices. The data scatter is due to device-to-device variation. In principle, all curves of Fig. 3.9 can be measured on one device, then the data scatter should be reduced or eliminated as demonstrated by the spectra obtained using the isochronal-EFSE technique in the next section which are very smooth since the measurement is made on one device during one measurement run. The key results in these transient-EFSE measurements on different devices are that all the data are clustered around an universal bell-shaped density of state curve, suggesting (i) the same traps are present in the different devices and

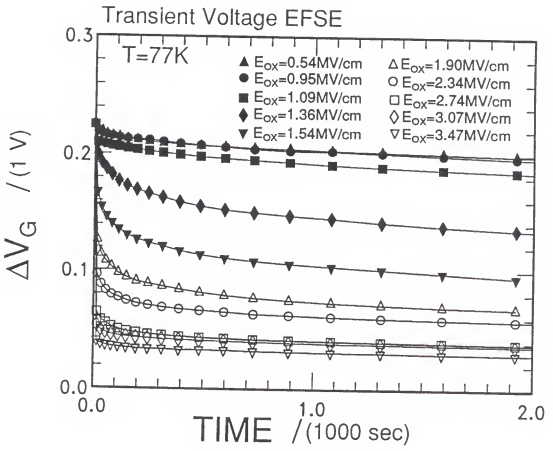

Fig. 3.9: At the start of the transient-EFSE technique, traps are charged by capturing electrons which are injected into the 184A dry/wet/dry (850C) oxide at the BiMOS injection conditions: $N_{INJ}=0.9x10^{14}cm^{-2}$, $E_{OX}=0.54MV/cm$, $J_{OX}=0.26\mu A/cm$, T=77K, and $V_{CB}=6.0V$. Gate voltage shift versus time for 10 values of the discharge-emission field.

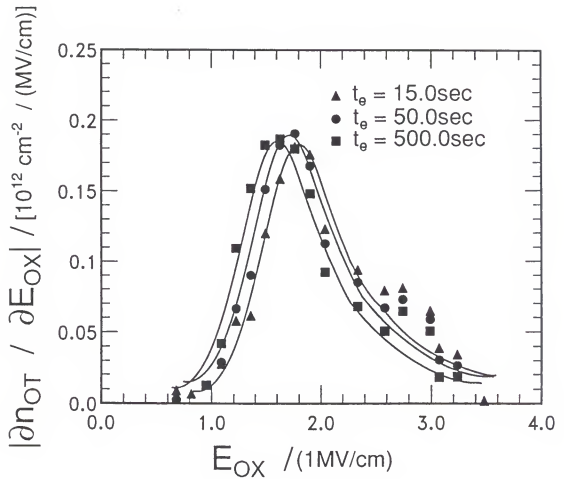

Fig. 3.10: $|\partial n_{OT}/\partial E_{OX}|$ evaluated at t_e equal 15.0, 50.0, and 500.0sec versus discharge-emission field.

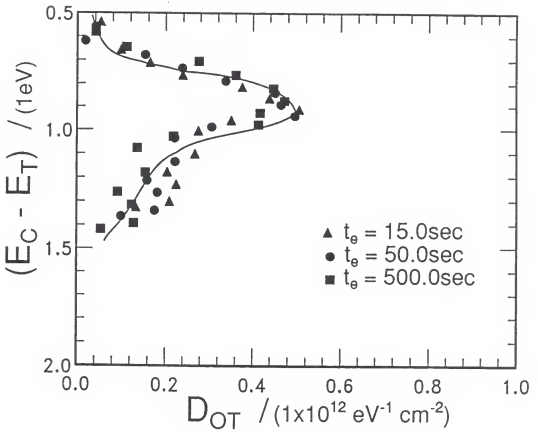

Fig. 3.11: Calculated density of states for the charged oxide traps.

(ii) using a different discharge-emission time t_e has little effect on the bell-shape of the data.

3.4-2 Isochronal-EFSE Applied to SiO_2

The isochronal-EFSE technique is applied to the thermally grown oxides. Electrons are injected into the oxide using the same BiMOS injection conditions in the previous section. After traps are discharged via electron tunnel emission for t_e seconds, ΔV_G is measured. The discharge field is increased by 0.1MV/cm and kept constant for t_e seconds, and then ΔV_G is measured again. The experiment is repeated using detrap-emission discharge times, t_e, of 5.0, 50.0, and 500.0 seconds. Figure 3.12 shows the gate voltage shift relative to the unstressed device measured after each discharge oxide field increment for t_e duration. $-\partial n_{OT}/\partial E_{OX} = |\partial n_{OT}/\partial E_{OX}|$ is calculated and plotted versus discharge field in Fig. 3.13. The centroid is assumed equal to the oxide thickness, $X_{OT}=X_{OX}$. The density of initially charged oxide traps is calculated from Eq.(3.9) and plotted in Fig. 3.14. A broad spectrum with a density peak between 0.9-1.0eV is observed. The broadness of the density spectra is characteristic of amorphous materials.

Recent theoretical calculations show that the lattice relaxes about an oxygen vacancy to enable the two silicon dangling bonds to form a 2.6 to 3.0A silicon-silicon bond [13]. Theoretical calculations for the $[(Si\text{-}O)_3{\equiv}Si \cdot \cdot Si{\equiv}(O\text{-}Si)_3]$ defect by Robertson[17-19], and Rudra and Fowler[13] give a shallow bound state at the neutral oxygen vacancy which is located at approximately 1.0eV below the oxide conduction band[15,16] and a 0.7eV±0.5eV thermal activation energy[13]. This is in good agreement with

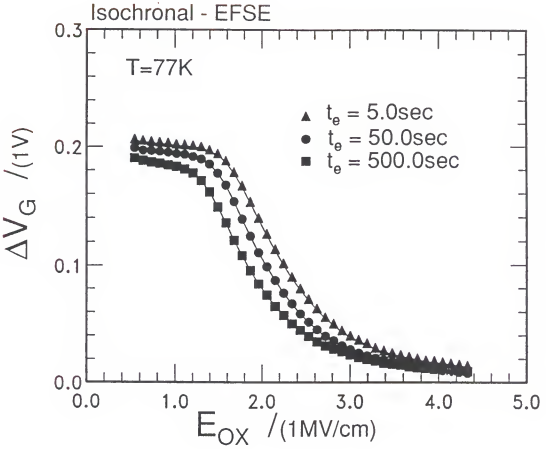

Fig. 3.12: Isochronal-EFSE technique where oxide traps are charged by electron capture at the same BiMOS injection condition as in Fig. 3.9. Gate voltage shift at the end of each t_e step versus discharge-emission field which is increased in 0.1MV/cm increments and maintained constant for t_e equal to 5.0, 50.0, and 500.0 sec.

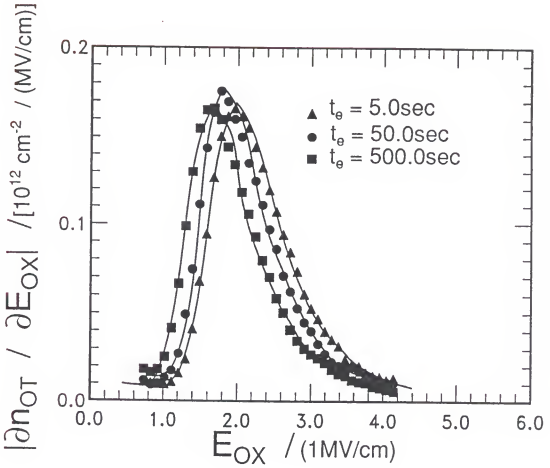

Fig. 3.13: $|\partial n_{OT}/\partial E_{OX}|$ versus oxide discharge field.

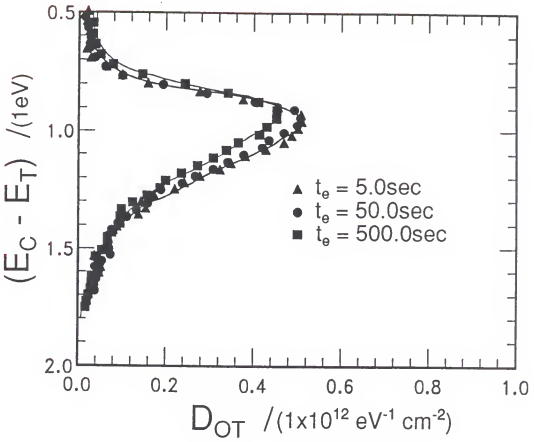

Fig. 3.14: Calculated density of traps.

our data. A range of silicon-silicon bond lengths is expected near the SiO_2 interface to give the observed broad spectrum.

3.4-3 Oxide Thickness Dependence of Trap charging

The density of charged oxide traps was calculated by assuming the trapped charge centroid equal to the oxide thickness, $X_{OT}=X_{OX}$. If the centroid is not equal to the oxide thickness, the density of charged oxide traps should be scaled by X_{OX}/X_{OT}. We apply the procedure of D. R. Young et al.[25] to our experiments to determine the centroid experimentally using a range of oxide thicknesses (93-281A) in dry 900C oxides. Figure 3.15 plots the gate voltage shift versus injected electron fluence due to charging electron traps at E_{OX}=1.1MV/cm, J_{OX}=1.3μA/cm^2, and 77K for oxide thickness of 93, 150, 201, and 281A. If the oxide traps were distributed uniformly throughout the oxide film and if the same trap density (#/cm^3) were present in all the 93 to 281A oxides, the gate voltage shift would vary with $1/X_{OX}^2$. However, if the oxide traps were located at the SiO_2/Si interface, the gate voltage shift would vary as $1/X_{OX}$. Figure 3.16 plots $\Delta V_G/X_{OX}$ versus fluence for the various oxide thicknesses which does not give the correct thickness dependence. A plot of $\Delta V_G/X_{OX}^2$ (not shown) also does not give the correct thickness dependence. Figure 3.17 plots $\Delta V_G/X_{OT}=\Delta V_G/(X_{OX}$-82A) where the centroid from the Si/SiO_2 interface, X_{OX}-X_{OT}, is taken to be 82A, i.e. $X_{OT}=X_{OX}$-82A from the gate/SiO_2 interface. This figure shows that the traps in the 150 to 281A oxides are all well represented by a single 82A centroid. The thinnest (93A) oxide result is also consistent, viz., it has a lower ΔV_G and it is not simply proportionally lower since there is an energy and spatial distribution of the trapped

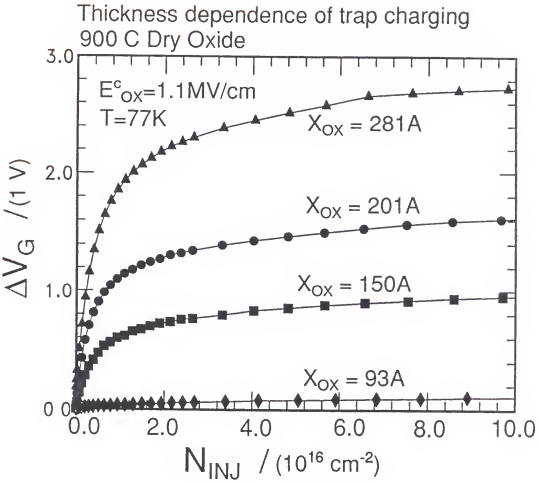

Fig. 3.15: Gate voltage shift versus electron fluence for 93-281A dry(900C) oxide.

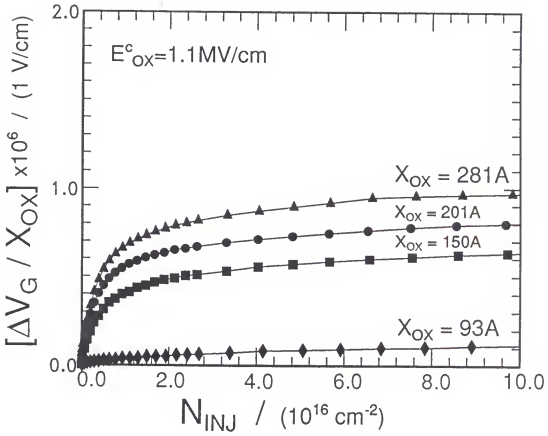

Fig. 3.16: Gate voltage shift divided by oxide thickness versus fluence.

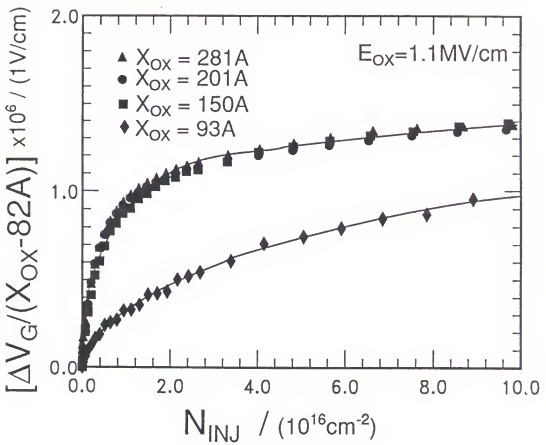

Fig. 3.17: Gate voltage shift divided by the oxide trap centroid versus fluence, $\Delta V_G/(X_{OX}\text{-}82A)$. BiMOS injection conditions: E_{OX}=1.1MV/cm, J_{OX}=1.3μA/cm, T=77K, and V_{CB}=6.0V.

electrons tunneling out of the trap during the 1.1MV/cm charging of the traps. This result is also consistent with the 90A centroid reported by Young, et al. of IBM [25] and others[26]. Their MOS capacitors had 162 to 715A thick dry 1000C oxides with aluminum gate, POA (post-oxidation anneal) of 1 hr at 1000C in N_2, and PMA (post-metallization anneal) of 20 minutes in N_2, and they were stressed by avalanche electron injection at 77K. Figure 3.18 plots the density of charged oxide traps in the 150 and 281A oxide after N_{INJ}=0.6x10^{16}cm^{-2} electrons are injected at E_{OX}=1.1MV/cm, and J_{OX}=1.3μA/cm^2, for 7.39x10^2 seconds at T=77K. The isochronal-EFSE measurements were made at t_e=30 second detrap-emission time for each 0.1MV/cm oxide field increment. When a centroid of 82A is used, nearly identical energy spectrum of the density of charged traps (magnitude and width) is found in the oxides with thicknesses of 150, 201, and 281A as indicated in Fig. 3.18. This is strong evidence that dry oxides greater than 150A have (1) the same energy spectrum of the density of charged and neutral traps and (2) the same spatial distribution of oxide traps. It is further supported by the IBM data of D. R. Young [25] on many differently processed thick oxides just cited (162-715A, 1000C dry oxides with aluminum gate) who gave a centroid of 90A and no energy spectra since the density of state measurement techniques (this EFSE or other methods) were not available.

The thickness independence of the density of states probably results from the traps being near the Si/SiO_2 interface. Traps near the SiO_2 interface are expected to be similar in oxides with thickness greater than 100A (or the trap centroid$\geq$82A) since the atomic structure near the

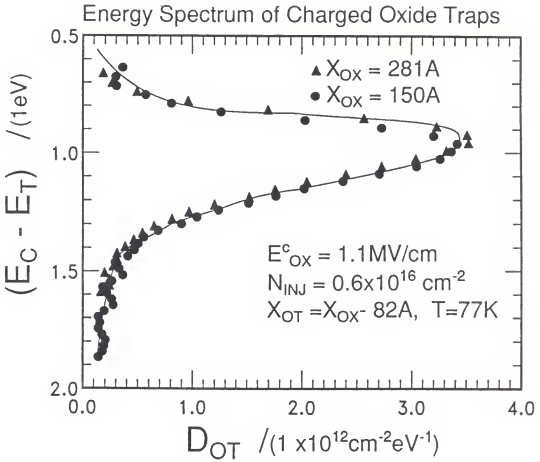

Fig. 3.18: Density of states for dry (900C) oxides of X_{OX}=281A and 150A. The oxide traps are charged by capturing electrons injected into the oxide at the BiMOS injection condition: N_{INJ}=6.0x10^{15}cm^{-2}, E_{OX}=1.1MV/cm, J_{OX}=1.3μA/cm, T=77K, and V_{CB}=6.0V.

interface is largely determined by the growth kinetics of the oxide on the single crystalline silicon [27].

In oxides with thickness less than 100A, a significant reduction in the density of electron traps is observed. This is to be expected since the centroid (~82A) is approaching the oxide thickness to cause significant trap-to-gate tunneling emission as predicted by Sah [28,3].

3.4-4 Reversibility of the Charging and Discharging Process

In this section, the reversibility of the charging and discharging process is demonstrated in one device by charging and discharging five times in order to show that the generation of new traps is negligible at low electric fields and that reproduceable recharging is possible. Electron traps are charged by injecting $N_{INJ}=0.9x10^{15}cm^{-2}$ electrons into the oxide at $E_{OX}=0.54MV/cm$ and T=77K. Next, D_{OT} is measured using the isochronal-EFSE technique at $t_e=50$ seconds and 0.1MV/cm oxide field increments. The maximum discharge field employed is 4.6MV/cm. During the measurement of the spectrum, all electron-filled traps shallower than 1.7eV below the oxide conduction band edge are detrapped. Figures 3.12, 3.14, and 3.18 showed that most of the trapped charge (~95%) at these BiMOS injection conditions are shallower than 1.7eV. The electron traps are charged and D_{OT} measured five more times at the same conditions. The charged trap density spectra are shown in Fig. 3.19 for the initial unstressed device and after the fifth cycle. The spectra are nearly identical. This near identity clearly shows that (1) the density of newly generated traps caused by (i) the electron transport though the oxide during charging and (ii) the capture of a conduction electron at the bound states in the oxide is much less

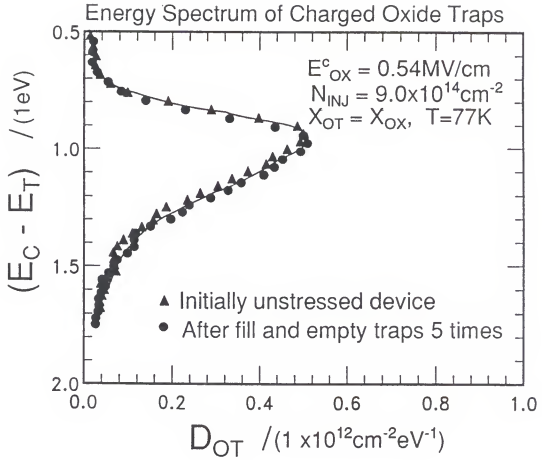

Fig. 3.19: Density of states for the electron charged oxide traps (1) initially unstressed device and (2) after traps are charged and discharged 5 times. The oxide traps are charged by electron injection into the oxide at the BiMOS injection condition: N_{INJ}=9.0x10^{14}cm^{-2}, E_{OX}=0.54MV/cm, J_{OX}=0.26μA/cm, T=77K, and V_{CB}=6.0V.

than the density of existing traps, and (2) the shallow traps (0.5-1.7eV) are not converted to an interface state[29] or a deep state [30,31] after electron capture as previously speculated. Oxide traps were also repeatedly charged with larger electron fluence. Again, nearly identical spectrum are observed.

3.4-5 Oxide Charge Altering the Applied Oxide Electric Field

The oxide electric field must be known accurately to evaluate the tunnel transition rate since the rate is very strongly (double exponential) dependent on the oxide electric field. The forgoing energy spectra were calculated by assuming that the oxide field is equal to the applied field (V_{OX}/X_{OX}) which is valid at low oxide charge densities. In this section, we show that this is a valid approximation for oxide charge density less than $2x10^{12}cm^{-2}$.

In order to evaluate the effect of the trapped charge on the local oxide electric field, the density of states for the charged oxide traps is measured after various injected electron fluences. The following experiment is performed on one device and reproduced in many devices: (1) a fraction of the electron traps are charged by injecting a fluence of electrons into the oxide ($N_{INJ} = 5.0x10^{14}cm^{-2}$); and (2) the energy spectrum of the charged traps is measured using the isochronal-EFSE technique. The oxide field is incremented between 1.2 to 4.6MV/cm and maintained constant for t_e=30 seconds at each increment. The procedure is repeated 25 times with increasing electron fluence injected into the oxide to charge a larger percentage of the traps. Figure 3.20 shows the gate voltage shift versus discharge oxide field for 10 of the cycles. Figures 3.21 and 3.22 show the energy spectrum for 16 of the cycles. The charged trap density, Q_{OT}, is

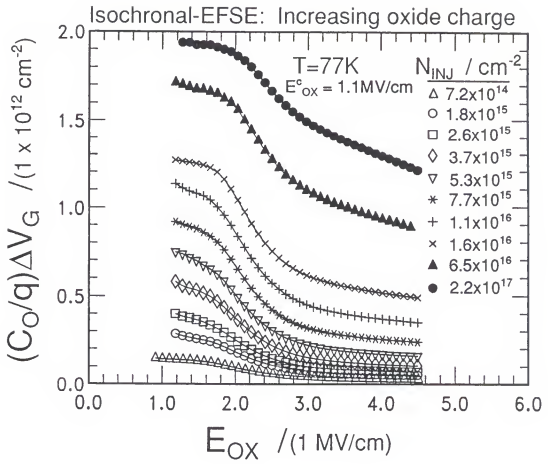

Fig. 3.20: Isochronal-EFSE applied to a MOS device with increasing amounts of oxide charge. Normalized gate voltage shift versus discharge-emission electric field. The oxide field is increased in 0.1MV/cm increments and maintained constant for 30 seconds. The oxide traps are charged by capturing electrons injected into the oxide at the BiMOS injection condition: E_{OX}=1.1MV/cm, J_{OX}=1.3μA/cm, T=77K, V_{CB}=6.0V, and N_{INJ} between 7.2x10^{14} and 2.2x10^{17}cm^{-2}.

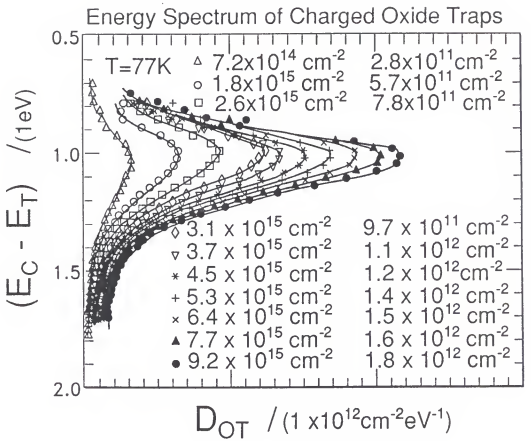

Fig. 3.21: Density of states of the charged oxide traps with increasing amounts of oxide charge. Same BiMOS injection condition as Fig. 3.20. Energy spectrum calculated using X_{OT}=X_{OX}. Q_{OT} between 2.8 to 18.0x10^{11}cm^{-2}.

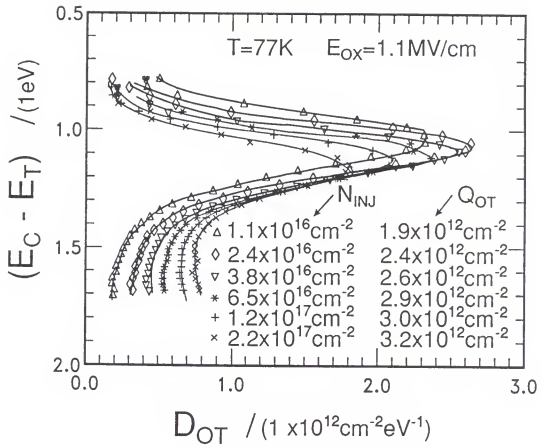

Fig. 3.22: Q_{OT} between 1.9 to 3.2.x10^{12}cm^{-2}.

labeled for each curve in Figs. 3.21 and 3.22. The charge is computed from the gate voltage shift using the X_{OX}-82A centroid measured previously. During a measurement of the density of states, traps shallower than 1.7eV will emit an electron when the largest discharge field (4.6MV/cm) is applied for 30 seconds. If there were traps deeper than 1.7eV that were charged, they did not emit an electron during the measurements. In Fig. 3.20, the gate voltage shift at 4.6MV/cm detrap-emission field continues to rise at higher cycles because filled traps deeper than 1.7eV are not detrapped during each cycle.

For the N_{INJ}=7.2 x $10^{14}cm^{-2}$ curve in Fig. 3.21, the oxide charge is small (Q_{OT}=2.8x$10^{11}cm^{-2}$). Hence, the spectrum is accurately calculated using E_{OX}=V_{OX}/X_{OX}. For larger density of oxide charge (up to 2x10^{12} cm^{-2}), the D_{OT} spectrum remains approximately the same shape, but its peak increases. There are small differences in the shape of these spectra which will be shown in the next section to be caused by the energy dependence of the capture cross section. The shallower traps in the spectrum have a larger capture cross section than the deeper traps.

When the negatively charged oxide trap density exceeds 2x$10^{12}cm^{-2}$, the shallower energy or upper shoulder of the spectra downshift to deeper energy as shown in Fig. 3.22. For example, the upper shoulder of the Q_{OT} = 3.2x10^{12} cm^{-2} curve downshifts to approximately 1.1eV. The downshift of upper shoulder for these curves is an evidence of significant alteration of the local electric field by the charged oxide traps. The increased local oxide electric field causes the tunnel emission rate at the shallower traps to increase significantly so that they could not be charged by electron capture.

The deeper traps (lower shoulder) are not affected as much and maintain essentially the same profile of density-of-charged-states.

3.4-6 Energy Dependence of the Capture Cross Section

The capture cross section as a function of electron trap energy is obtained in this section. The energy dependence of the cross section is observed in Figs. 3.21 and 3.22. The shallower traps in the spectrum have a larger capture cross section than the deeper traps. In Fig. 3.21, the density of states for the shallower part of the spectrum (around 0.9eV) saturates with increasing fluence at approximately $4.0 \times 10^{15} cm^{-2}$. However, the density of states for traps at 1.2eV does not saturate until a larger fluence of $1 \times 10^{17} cm^{-2}$. The kinetics for electron capture by a trap is

$$dn_{OT}(t)/dt = c_n^t n[n_{TT} - n_{OT}(t)] - (e_n^t + \omega_n) n_{OT}(t) - e_n^n n n_{OT}(t) \quad (3.10)$$

where we use the widely used notation convention due to Sah: n is the electron concentration in silicon dioxide (cm^{-3}), c_n^t is the thermal capture coefficient (cm^3/s), n_{TT} is the areal density of oxide traps, $n_{OT}(t)$ is the areal density of trapped electron(cm^{-2}), e_n^t is the field dependent thermal emission coefficient of trapped electrons (s^{-1}), ω_n is the Price-Sah trap-to-band tunneling emission rate, and e_n^n is the electron impact emission coefficient. Trapping kinetics at a single discrete level is usually applied to SiO_2. However, the observed trapping in these samples is due to a distribution of trap energies and not a discrete level. The coefficients (e_n^t,c_n^t, etc.) in Eq. (3.10) are highly sensitive to the energy level of the trap. The coefficients will vary over many orders of magnitude for trap energies

differing by a few tenths of an electron volt. For example, at higher fields at which the trap-to-band tunnel emission term in Eq. (3.10) becomes important and then dominates, the coefficient varies nearly 10 orders of magnitude for trap energies across the spectrum shown in Fig. 3.14 or Fig. 3.18. Therefore, the kinetic equation governing electron (or hole) trapping must be written for a distribution of traps in energy. The charging-capture kinetic equation for the density of electron-charged oxide traps, D_{OT}, is

$$dD_{OT}(t,E_T))/dt = c_n^t(E_T)\,n[D_{TT} - D_{OT}(t,E_T)] \qquad (3.11)$$

where D_{TT} is the total density of oxide traps and the emission terms are neglected. The tunnel and thermal emission rates are negligible at this low field (less than 1.1MV/cm) and low temperature (77K) injection condition[12]. Impact emission is not important below the threshold field of electron heating, 1.5MV/cm [32]. As a further test on whether the emission terms are important under these injection conditions, the traps are charged using different oxide current densities(J_{OX}=0.25μA/cm^2 to 2.5μA/cm^2) and one charging oxide field E_{OX}=1.1MV/cm. Nearly identical spectra of charged traps are observed. This indicates that tunnel, thermal, and impact emission processes are not important or their rate are low compared with the capture rate during charging at low oxide fields and low temperatures.

To solve the kinetic equation, the thermal velocity is approximated by the drift velocity using $J = qnV_D = qn\Theta$. This was shown to be a valid approximation at the low oxide fields used [33]. The density of charged oxide traps as a function of charging-capture time or injected fluence is

$$D_{OT}(t,E_T) = A \{ 1 - \exp[-\sigma_n^t(E_T)N_{INJ}] \}. \qquad (3.12)$$

where the thermal capture cross section is defined phenomenologically as $\sigma_n^t = c_n^t/\Theta_n$. The density of charged oxide traps versus electron fluence is plotted in Fig. 3.23 for several values of trap energy obtained from Figs. 3.21 and 3.22. Figure 3.23 shows that the shallower traps are charged up by electron capture faster than the deeper traps. This is consistent with the notion that shallow traps have a larger electron capture cross section. The curves in Fig. 3.23 are least-squares fitted accurately to the one-time constant model, Eq. (3.12), and give the capture cross section at each trap energy. Figure 3.24 plots these capture cross sections versus the trap energy level. It shows that the capture cross section decreases two orders of magnitude, $\sigma_n^t = 10^{-15}$ to 10^{-17} cm^{-2}, in the energy range 0.8 to 1.7eV. This range of the capture cross sections is consistent with the empirically average values reported in the literature[30,31,34]. However, our results show for the first time that there exists a continuous distribution of capture cross sections due to a continuous distribution of trap energy levels and not several discrete traps as previously assumed [30]. A distribution is expected in an amorphous solid since it has continuously varying atomic environments around the defects associated with the oxide traps.

The energy dependence of the capture cross section and the broad energy spectrum of traps now offers the reason why the gate voltage shift versus fluence curve given in Fig. 3.15 and reported in the literature [15,30,31] does not follow a simple one-exponential model. The curves are

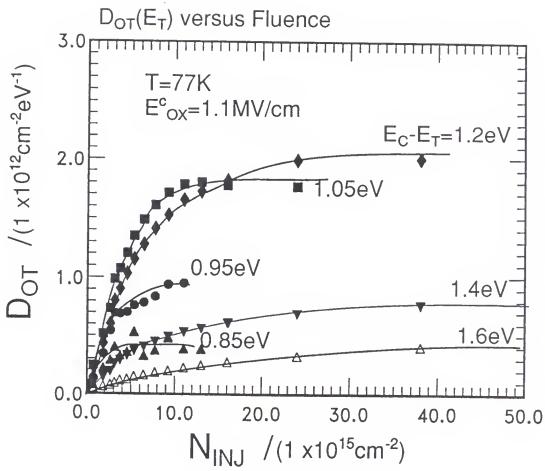

Fig. 3.23: $D_{OT}(E_T)$ versus injected electron fluence at E_T=0.85, 0.95, 1.05, 1.2, 1.4, and 1.6eV. Same BiMOS injection conditions as Fig. 3.20.

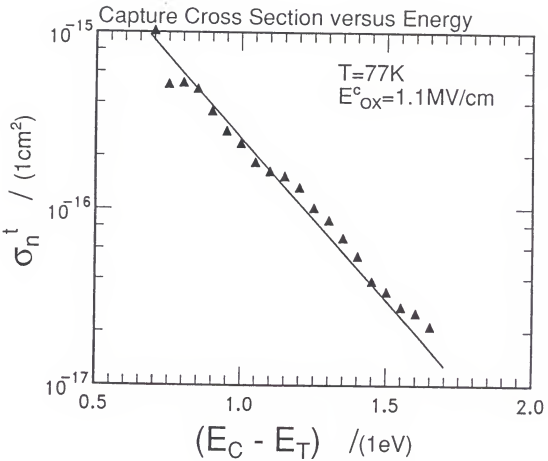

Fig. 3.24: Electron capture cross section versus trap energy level. The cross section is obtained by a least-squares one exponential fit to the curves in Fig. 3.23.

frequently least-squares fitted to two or more exponential terms whose empirical fit parameters (time constant and amplitude) depend on the fluence range selected by the researchers because deeper levels with smaller capture cross sections will begin to appear in the ΔV_G shift only in the higher fluence range. Furthermore, the ΔV_G-t or ΔV_G-N_{INJ} curves do not saturate at higher fluence (in the range $N_{INJ} > 1.0 \times 10^{16} cm^{-2}$) and the rise slows down which is a further indication of the presence of the deeper oxide traps with smaller capture and emission cross sections. For example, in our samples just described, nearly all the traps shallower than 1.5eV are charged after $N_{INJ}=1.0x10^{16} cm^{-2}$ at 77K. However, traps deeper than 1.5eV with smaller capture cross sections are not charged until larger injected electron fluences.

3.4-7 Form of the Tunneling Transition Rate

All energy spectra were calculated using $W^2=10^{-24} V^2 cm^{-3}$ and $m_x=m_y=m_z=m_o$ where m_o is the free electron mass. In this section, the sensitivity of the measured energy spectrum on the energy dependence of the pre-exponential factor and effective mass is investigated. Sensitivity from both are expected to be small again to the double exponential.

3.4-7a Pre-exponential factor

In the Price-Sah model for the tunnel transition rate, the pre-exponential factor has an electric field dependence to the first power (E_{OX}^1). Chaodhuri, Coon, and Karowasiri (to be referred to as CCK) derived a 3-dimensional expression which has a E_{OX}^{2n-1} dependence [35]. The transition rate in the CCK model is

$$\omega = \omega_o (\alpha/E_{OX})^{2n-1} \exp(-\alpha/E_{OX}) \tag{3.13}$$

where

$$\alpha = \frac{4(2m^*)^{1/2} E_T^{3/2}}{3q(h/2\pi)} \tag{3.14}$$

$$\omega_o = \frac{6^{2n} E_T |s(n)|^2}{3(h/2\pi)\Gamma^2(n+1)} \tag{3.15}$$

and

$$s(n) = [\pi/(\sin(n\pi))] \left[(1/2) \sum_{m=0}^{m=\infty} (n-m-1)^{-2} (n-m)^{-2} \right]^{1/2} \tag{3.16}$$

The parameter n(0→1) takes into account the nature of the trap binding potential, i.e. whether a trap is shallow, deep, charged, or neutral. For neutral or deep traps used in the Price-Sah model [22], n is close to zero. For shallow coulombic centers, n is close to one [36]. To test the sensitivity of our result on n, the energy spectrum for the isochronal-EFSE measurement with 50 second detrap-emission time in Fig. 3.14 is analyzed using values of n ranging from zero to one. The results are plotted in Fig. 3.25.

As seen in Fig. 3.25, the EFSE technique is not very sensitive to the value of n. The peak in the spectrum varies at most by 0.18eV at 0.9eV for n ranging from its maximum (n=1) to minimum (n=0). For oxide traps in this study, electrons are captured by neutral centers. The initial charge state of the traps, neutral, is obtained by comparing the C_G-V_G curve on an unstressed device to the theoretical curve. Thus, n should be close to zero as in the Price-Sah model.

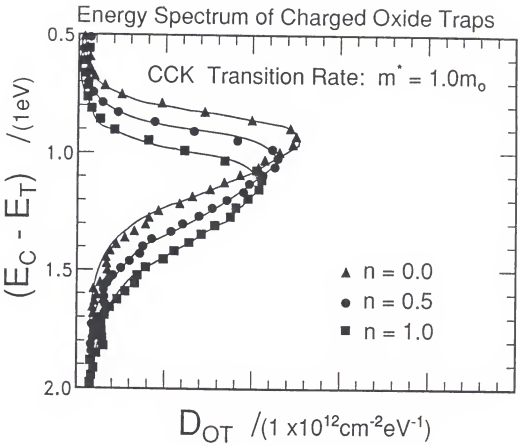

Fig. 3.25: Density of states is calculate from t_e=50sec. tunneling emission data in Fig. 3.12 using Chaodhuri, Coon, and Karowasiri tunneling transition rate n varied between 0 to 1.

The matrix element of $10^{-24}V^2cm^3$ (from the gold center in Si)[12,22] is consistent with n=0.22.

3.4-7b Effective mass

Throughout the paper, the spectra were calculated using an effective mass, m^* ($=m_x=m_y=m_z$), equal to the free electron mass, m_0. The sensitivity of the density of states on the effective mass is investigated in this section. Numerous values for the effective mass in SiO_2 have been obtained from band-to-band (interband) Fowler-Nordheim (FN) tunneling current measurements using electron injection from both the metal gate and Si-substrate into the oxide conduction band. A range of values for the effective mass from $0.3m_0$ to $1.0m_0$ have been reported [37]. Most of the reported FN tunneling data seem to suggest $m^*=0.5m_0$ [37].

The effective mass characterizing trap-to-band transitions in the oxide should be different from the effective mass measured in band-to-band FN tunneling experiments for the following two reasons. First, the band-to-band tunneling experiments measure the effective mass within 20-30A of the SiO_2/Si interface or gate/SiO_2 interface. Since both interfaces are strained, the dispersion (E-k) relationship in the SiO_2 will be altered, thus changing the effective mass. For example, the first several monolayers of SiO_2 near the SiO_2/Si interface are denser (shorter Si-Si bond) and have a different structure than bulk amorphous SiO_2 [27]. However, from the data in the literature, strain alteration of the effective mass at the interface does not appear to have been included as a large effect. Gate metal electrodes deposited at low temperatures did not seem to significantly strain the oxide near the gate/oxide interface as compared to the oxide 20-30A within the SiO_2/Si interface [38]. FN

tunneling electron injection from the metal gate and Si substrate both give approximately $m^*=0.5m_o$ [37]. Second, in FN tunneling experiments, the effective mass through the forbidden path lies in a deeper energy range in the SiO_2 energy gap than the trap-to-band tunneling (~0.5→1.7eV) in this paper due to the larger SiO_2/Si (~3eV) and metal/SiO_2 (~3eV) barrier. It is not unexpected that the parabolic dispersion relationship may not hold throughout the entire SiO_2 energy gap (9eV) or even the upper 1/3 near the oxide conduction band edge with the consequence of varying effective mass with energy or position along the forbidden path. Maserjian suggested that FN tunneling may have two channels via a heavy ($m^*=.85m_o$) and a light ($m^*=0.27m_o$) oxide conduction band [38]. The FN effective mass is then an effective mass averaged over this energy range if the separation of these two band edges is zero or extremely small, otherwise, only the lowest oxide conduction band edge dominates, a more likely case since the tunneling emission rate is so strongly dependent on the energy level (double exponential). Furthermore, photon-assisted FN tunneling data of Weinberg and Hartstein suggested that the effective mass is constant ($m^*=0.5m_o$) throughout a shallow energy range (0.5 to 1.5eV) [39].

Figure 3.26 analyzes the isochronal-EFSE data for the 50 second time step using effective mass values from $0.5m_o$ to $1.0m_o$. Uncertainty in the effective mass gives a small uncertainty in the location of the peak in the density of states. Depending on the value of the effective mass used, the peak shifts from 1.0eV ($m^*=m_o$) to 1.3eV ($m^*=0.5m_o$). Therefore, the results in this paper are not strongly affected by the value of the effective mass used.

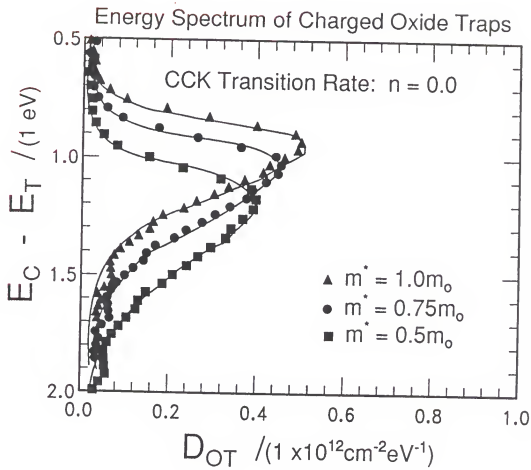

Fig. 3.26: The effective mass varied between 0.5 to 1.0 times the free electron mass.

Nevertheless, the effective mass must be cited in order for the result to be useful in MOS reliability design applications.

3.5 Conclusion

Two new EFSE techniques, the transient- and the isochronal-EFSE, are described and analyzed in detail. Comparison with the exact transient-EFSE shows that the faster isochronal-EFSE gives accurate result. Both methods require large scale computer-controlled 5-6 significant figure data acquisition system and long-time (100-hour) data acquisition runs. The methods are used to measure for the first time the energy spectrum of the oxide electron traps in pure SiO_2 film on VLSI grade crystalline silicon. Electron traps are found to be distributed throughout the upper SiO_2 energy gap between 0 to at least 3.0eV below the conduction band edge. A broad energy spectrum with a density of states peak between 0.9-1.0eV below the conduction band edge is observed in all dry oxides used in the experiments. The electron capture cross section of the traps varies exponentially with trap energy depth. Shallower traps have a larger cross section than the deeper traps, decreasing from 10^{-15} to 10^{-17} cm^{-2} in the energy range of 0.5 to 1.7eV below the conduction band edge. Several error analyses are presented to show that the EFSE technique is a powerful new and accurate technique to characterize electron (and hole) trapping kinetics and parameters in SiO_2 and other insulators. The analytical expressions derived for the EFSE technique are highly accurate and valid for traps at a discrete energy level or a distribution of levels. Furthermore, the technique has great experimental facility because of the ease in controlling the

oxide electric field compared with controlling temperature in the thermally stimulated methods or photon energy in the optically stimulated methods. Furthermore, the fundamental data obtained from varying the electric field stimulant is directly applicable to the reliability design of current and future generations of submicron integrated circuits, as demonstrated by the illustrations given in this chapter, without having to translate and extend the fundamental data and parameters empirically to those used in engineering designs of reliability VLSI transistors.

CHAPTER 4
TUNNELING AND THERMAL EMISSION OF ELECTRONS FROM A DISTRIBUTION OF SHALLOW TRAPS IN SIO_2

4.1 Introduction

In Chapter 4, the charging of existing oxide electron traps is found to be strongly oxide electric field dependent. The transition rate of trapped electrons tunneling into the oxide conduction band increases exponentially with increasing oxide field due to barrier thinning. Electron detrapping via tunnel emission is measured at 77K using the isochronal electric-field-stimulated emission technique presented in Chapter 3. This technique gives the energy spectrum of the charged oxide electron traps. The spectrum of charged oxide traps is measured at oxide fields between 1 to 4MV/cm and temperatures between 77 to 294K. The experimental spectrum peaks at 0.9eV for low temperature and low oxide field while the measured thermal activation for electron detrapping is about 0.4eV. The energy level and thermal activation energy are consistent with the Mott ratio of the Jahn-Teller effect for the polar SiO_2, 1.9.

Previously, increased electron trapping has been reported in SiO_2 at 77K[25,34] with an 0.3eV activation energy for the thermal emission of electrons from these oxide traps[34]. In this chapter, we measure for the first time the energy distribution of these shallow oxide traps charged at

oxide field between 1 to 4MV/cm and temperatuers between 77 to 294K. very-large-scale-integrated (VLSI) oxides obtained using the new isochronal electric-field-stumulated emission technique.

4.2 Experimental Method

Electron are injected into the oxide by the forward-biased substrate emitter-base n+/p junction of a vertical n+/p/n-inversion-layer composite bipolar metal-oxide-semiconductor (BiMOS) transistor [21]. The gate oxides were grown on a p-well in Si using three oxidation processes, 850C dry/wet/dry, 900C dry, and 950C partial steam. Poly-crystalline silicon gate is then deposited on the SiO_2 and doped n-type by $POCl_3$. The self-aligned source and drain were implanted with $1.0 \times 10^{15} cm^{-2}$ of 100KeV phosphorus ions. The implantation damage was annealed at 850C for 30 minutes. The source and drain were then diffused at 950C for 90 minutes in nitrogen ambient. High purity aluminum was then thermally evaporated and patterned to form the ohmic contacts.

Electrons are injected into the gate oxide at low oxide fields, 1 to 5MV/cm, to charge the existing oxide traps. Generation of new oxide electron traps is minimized by limiting the electron stress to this low field range[23,24]. The electron injection is periodically stopped to measure the gate capacitance versus gate voltage (C_G-V_G) and drain current versus gate voltage (I_D-V_G) curves at the stress temperature. Parallel positive gate voltage shift of the C_G-V_G and I_D-V_G is observed which indicates

charging of existing oxide electron traps[23] and not the generation of new interface traps. The identical gate voltage shift of the I_D-V_G and C_G-V_G curves indicates uniform charging of oxide traps because the I_D-V_G curve is sensitive to oxide charge localized near the source while the C_G-V_G curve is sensitive to oxide charge along the entire channel.

4.3 Temperature and Oxide Field Dependence of Oxide Trap Charging

Figure 4.1 shows the oxide electric field dependence (1.3 to 4.6MV/cm) of the gate voltage shift, measured at 1.0μA drain current and 100mV drain to source voltage, versus electron fluence at 77K. Figure 4.2 shows the stress temperature dependence (77, 150, 210, and 294K) of the gate voltage shift at 2.1MV/cm oxide field. The saturation of the gate voltage shift after an injected electron fluence greater than $2x10^{16}$ cm^{-2} is due to the steady-state balance of the field and temperature dependent charging and discharging processes of the oxide traps. The saturation indicates negligible generation of charged new oxide traps[23]. The decrease in the saturated gate voltage shift at a constant temperature (77K) in Figure 4.1 corresponds to a decreasing density of charged oxide traps with increasing oxide electric field. The decrease in the saturated gate voltage shift at a low constant oxide field (2.1MV/cm) in Figure 4.2 corresponds to a decreasing density of charged oxide traps with increasing temperature. The decreases are due to the exponentially increasing tunnel emission rate with increasing oxide electric field (Fig. 4.1) and exponentially increasing thermal emission rate with increasing temperature (Fig. 4.2).

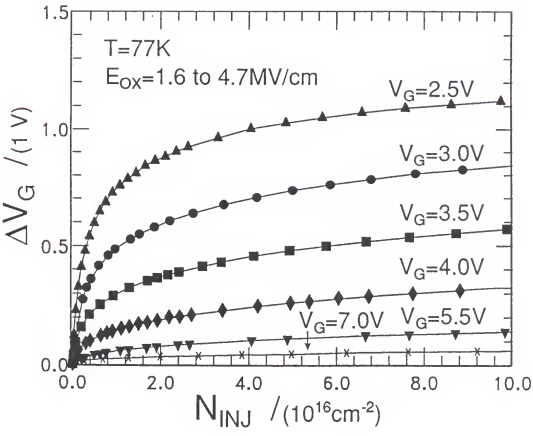

Fig. 4.1: Gate voltage shift versus injected electron fluence for 150A dry/wet/dry (850 C) oxide and gate voltages (V_G) between 2.5-7.0V and substrate injection stress: T=77K, source and drain/base reverse bias (V_{CB}) 6.0V, gate current (I_G) 5.0nA.

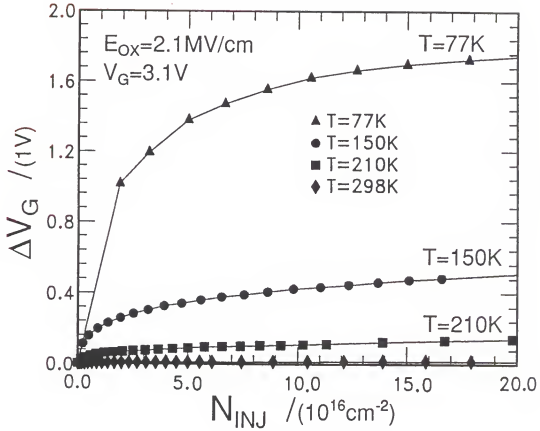

Fig. 4.2: Gate voltage shift versus injected electron fluence for 150A dry/wet/dry (850 C) oxide and temperatures between 77-294K and substrate injection stress: V_G=3.1V, V_{CB}=6.0V, I_G=100nA.

The importance of tunneling emission[14] in SiO_2 has been recognized recently but no experimental data were reported[14]. We use the isochronal electric-field-stimulated emission technique to characterize tunneling emission of electrons from oxide traps. This technique consists of the following steps: (1) the oxide electron traps are first charged at a constant temperature and low oxide electric field by electron injection into the gate oxide, (2) the electron injection is stopped and the BiMOS is cooled to 77K, (3) the oxide electric field (discharge field) is increased in 0.1MV/cm steps and maintained constant for 300 seconds at each step, and (4) at the end of each 300-second step, the gate voltage at a drain current of 1.0μA is measured to record the differential oxide detrapping via tunneling emission of the electrons trapped at the oxide traps.

The electron traps in the three oxides were first charged at 77K and a low oxide electric field (1.2MV/cm), and then discharged by increasing the oxide electric fields in steps. Figure 4.3 shows the gate voltage shifts from the unstressed value versus discharge oxide electric field. The gate voltage shift decreases for increasing discharge oxide field as the electrons are detrapped. The curve has a maximum slope at a discharge oxide field of approximately 2.0MV/cm which occurs when the largest number of electrons are detrapped in a unit energy range.

The energy spectrum of the oxide traps is calculated from the experimental data using the Price-Sah tunneling emission model[22] which gave a tunneling emission rate of

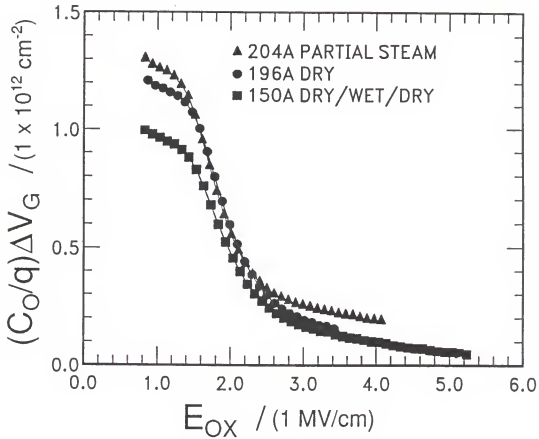

Fig. 4.3: $(C_O/q)\Delta V_G$ measured at the end of each 300 second discharge versus average discharge oxide electric field for 204A partial steam (950 C), 196A dry (900 C), and 150A dry/wet/dry (850 C) oxides. Substrate injection at 77K to fill traps: V_{OX}/T_{OX}=1.2MV/cm, I_G=5.0nA, injection time (T_{INJ}) 2000s.

$$\omega = (\pi^2/h^3)(m_y m_z)^{1/2}(E_{OX}/E_T)W^2 \exp(-2\Theta) \quad (4.1)$$

$$\text{where } \Theta = (4\pi/3)(2m_x)^{1/2}E_T^{3/2}/(hE_{OX}) . \quad (4.2)$$

E_{OX} is the oxide electric field. E_T is the energy level of the oxide electron trap measured from the oxide conduction band. W^2 is the square of the tunneling transition matrix element. As shown in Chapter 3, the density of states is computed from

$$D_{OT}(E_{Ti}) = [\Delta N_{OTi} - \Delta N_{OTi-1}] / [E_{Ti} - E_{Ti-1}]$$

$$= (C_O/q)[\Delta V_{Gi-1} - \Delta V_{Gi}] / [E_{Ti} - E_{Ti-1}] \quad (4.3)$$

where E_{Ti} is computed from $\omega_{1i}t=1$ at each i-th experimental E_{OXi}.

The energy spectrum for the existing oxide traps, D_{OT} vs. E_T, charged at 77K and oxide field of 1.2MV/cm is the top curve (triangular marker) shown in Figures 4.4 and 4.5 for the dry/wet/dry oxide. The partial steam and dry oxides gave the same spectra. We used $W^2=10^{-24}V^2cm^3$[22] and $m_x=m_y=m_z=m_o$. The sensitivity to the numerical value of W^2 used is 0.9eV ± 0.1eV for the peak when W^2 is increased or decreased by two orders of magnitude. If the band-to-band (Si to SiO_2) tunneling electron mass reported by Weinberg[40], $m_x=m_y=m_z=0.5m_o$, is used for this trap-to-band tunneling process then, the peak shifts to 1.2eV.

Figure 4.4 shows the field dependence (1.2, 1.5, 1.7, 1.8, and 2.0MV/cm) of spectra of the charged oxide electron traps which reaches an asymptotic shape at the lowest oxide electric fields, 1.2MV/cm. Since

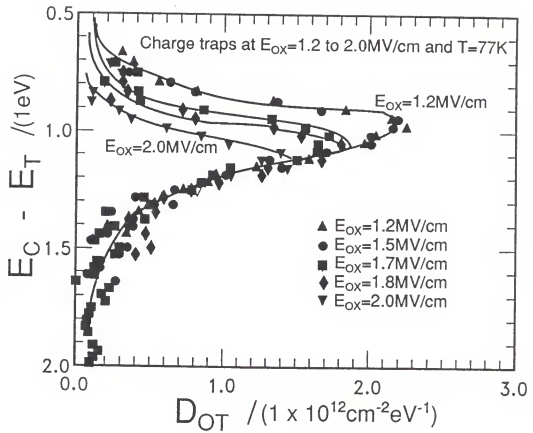

Fig. 4.4: Density of charged oxide electron traps, ρ_{OT}, versus energy for 150A dry/wet/dry (850 C) oxide. Substrate injection at gate voltages (V_G) between 1.85-3.0V to fill traps: T=77K, I_G=5.0nA, V_{CB}=6.0V, and T_{INJ}=2000s.

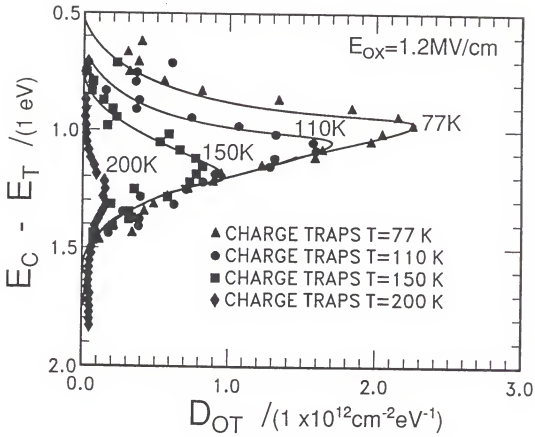

Fig. 4.5: Density of charged oxide electron traps versus energy for 150A dry/wet/dry (850 C) oxide. Substrate injection at temperatures between 77-200K to fill traps: V_G=1.85V, I_G=5.0nA, V_{CB}=6.0V, and T_{INJ}=4000s.

thermal emission at 77K is negligible for traps with thermal activation energy greater than about 0.1eV (emission rate dropped by $e^{(-0.10/0.006)} = 10^{-10}$), the energy spectrum at the lowest field (1.2MV/cm) is essentially the spectrum of the total oxide electron traps.

Figure 4.5 shows the temperature dependence (77, 110, 150, and 200K) of the spectra of charged oxide traps at the lowest oxide field. The decrease in charged traps with increasing temperature is due to thermal emission. The fraction of oxide traps charged at a given temperature is $(1+e_n q/\sigma_n J)^{-1}$ where σ_n is the electron capture cross section, J is the oxide current density, and e_n is the thermal emission rate. The 60% reduction in trapped charge from 77 to 150K in our data give a thermal activation energy for electron detrapping of about 0.4eV, using $J=1.3\mu A/cm^2$, $\sigma=10^{-16}cm^2$ (from Figures 4.1 and 4.2), and a thermal emission preexponential frequency factor of $10^{10}s^{-1}$. This is consistent with the 0.3eV peak of the thermal activation energy spectrum measured by Ning[34]. The 0.1eV lower value reported by Ning may be due to Poole-Frenkel barrier lowering by the oxide electric field employed by Ning.

Our measured 0.9eV trap depth from tunneling is larger than the thermal activation energy, 0.4eV. The difference is due to lattice relaxation during thermal activation, i.e. the Jahn-Teller effect, according to the Franck-Condon principle which also applies to tunneling. Lattice relaxation during thermal detrapping at point defects and impurity centers is small in non-polar covalent semiconductors (< 5meV in Si[41]), moderate in polar covalent semiconductors (60meV for Cr in GaAs[42]), and largest in ionic crystals (1eV for the $^1S_0$ to $^3P_1{}^o$ transition at Tl impurity in KCl[43]).

Mott[20] showed that the ratio of the optical ionization energy to thermal activation energy (E_o/E_{th}) is equal to the ratio of the static to high-frequency dielectric constant. The theoretical Mott ratio is about 2.0 in ionic crystals and 1.9 in SiO_2. Our data gives a ratio of 0.9/0.4 = 2.2. Experimental lattice relaxation energy data in SiO_2 is scarce. In order to account for the 5.8eV absorption associated with the neutral trivalent defect (Si_3^o), O'Reilly and Robertson[16] and Griscom[44] proposed that the Si_3^+ defect relaxes 3eV after capturing an electron giving a Mott ratio of 5.8/(5.8-3.0)=2.1. A 3.3eV lattice relaxation was proposed by O'Reilly and Robertson[16] and Gee and Kastner[45] to explain the 7.6eV absorption band in SiO_2 that gave the 4.3eV photoluminescence[45], giving a Mott ratio of 7.6/4.3=1.8.

4.4 Conclusion

In summary, charging SiO_2 traps by electrons is strongly dependent on oxide electric field due to the exponentially increasing tunneling detrapping rate with increasing oxide electric field. The isochronal electric-field-stimulated emission technique is used to give the energy spectrum of the charged oxide traps. It is found that the oxide electron traps are distributed in energy with a peak at 0.9eV and a thermal activation energy of about 0.4eV for electron detrapping. The oxide electric field and temperature during electron trapping is shown to alter the energy spectrum of the charged oxide trap or trapped electron density. Both the tunneling and thermal emission rates of electrons bound at shallow traps are high at

high fields and temperatures. Thus, only deeper oxide traps are charged by injected electrons at high oxide electric fields and temperatures.

CHAPTER 5
POSITIVE CHARGE GENERATION IN SiO_2 BY ELECTRON-IMPACT-EMISSION OF TRAPPED ELECTRONS

5.1 Introduction

In Chapter 5, experiments are presented which indicate for the first time that the positive charge located in the bulk oxide film probably results from creation of the E′ center, V_O^+ donor, due to emission of a trapped electron by electron impact at an initially neutral bridging oxygen vacancy V_O, $[(Si\text{-}O)_3{\equiv}Si\cdot \cdot Si{\equiv}(O\text{-}Si)_3]$. An impact electron threshold energy of 7eV for positive charge generation is measured. A shallow neutral oxide electron trap located 1eV below the conduction band is also measured on the same samples which becomes negatively charged after capturing an electron. An increase in the density of the shallow trap and a higher positive charge generation rate at the deeper trap are observed in samples annealed in nitrogen at 800-1000C which are oxygen deficient and consistent with the bridging oxygen vacancy model. The measured shallow (1eV) and deep (7eV) levels are in good agreement with the theoretical bound state energies for the bridging oxygen vacancy, about 1eV for the neutral shallow bound state and 7.8eV for the positively charged deep bound state. The electron impact emission coefficient of trapped electron is found to be $\alpha{=}3500cm^{-1}exp(-33MVcm^{-1}/E_{OX})$. Electron capture at the deep positive

trap, $V_O^+ + e \rightarrow V_O$, limits the buildup of positive oxide charge during electron impact. The electron capture cross section is found to be proportional to E_{OX}^{-n} (n=2 to 4 and E_{OX}=0.6 to 7.0MV/cm).

Previous studies have shown that electron transport in SiO_2 at high electric fields generates positive oxide charge[46-64] known as "anomalous positive charge." This phenomena has been observed in both metal and poly-Si gate metal/oxide/semiconductor capacitors(MOSC)[46]. It is technologically important because it occurs at high electric fields prior to breakdown[65-67] in integrated-circuit grade oxides. The mechanism of positive charge formation is not well understood although numerous models have been proposed[47-55]. These and other models are illustrated in the transition energy diagram[4] in Figure 5.1 such as transitions (1), (2), (3), (4) followed by (9), (5) followed by (11), (6), and others. It has been speculated that the positive charge comes from holes generated by energetic electrons[47-50]. These holes can subsequently be trapped in the bulk oxide film [transition (11)], trapped near the SiO_2/Si interface [transition (9)], or after passing through the oxide continue on into the silicon substrate to give the hole substrate current. Hole generation by interband electron impact was proposed by Klein and Solomon[47] [transition (5)]. Hole injection from the anode [transition (4)] via surface plasmon was proposed by Fischetti, Weinberg and Calise[48]; via exciton decay proposed by Weinberg and Rubloff[49]; or via tunneling injection of energetic hole created by the energetic electron proposed by Weinberg, et. al. [50]. Doubts were raised on hole transport from the gate into the oxide to explain the substrate hole current observed at very low temperatures (as low as 20K)[64] because hole

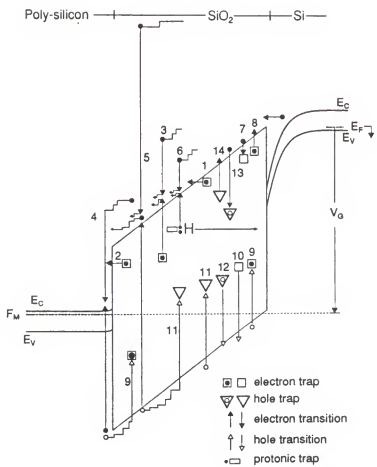

Fig. 5.1: Transition energy diagram illustrating the mechanisms of positive oxide charge generation at high oxide fields: (1) and (2) trap-to-band tunneling emission from an initially neutral oxide trap, (3) Emission of trapped electron by electron impact emission, (4) hole injection from the gate-conductor, (5) band-to-band electron impact emission, and (6) breaking a hydrogen bond in the oxide with the released hydrogen migrating away to the SiO_2/Si interface. Transitions (7) through (10) are the four transitions at an electron trap: (7) electron capture, (8) electron emission, (9) hole capture, and (10) hole emission. (11) through (14) are analogue transitions for a hole trap. After Chih-Tang Sah, Fundamentals of Solid-State Electronics, World Scientific Publishing Co. 1991 Figs. 684.1 and 684.2 on pages 675 and 677[4].

transport is a thermally activated process and found to be suppressed at low temperatures by Hughes[68]. Sah, Sun and Tzou have shown a large positive oxide charge generation in wet oxides and oxides rinsed by deionized water which led them to suggest a chemical reaction involving hydrogen near the SiO_2/Si interface[51-53].

It is possible that the varied conditions of positive charge generation previously reported were related to the many possible generation mechanisms which are highly dependent on the sample preparation and stress conditions. The experimental data in the literature on positive oxide charge generated by electrons can be classified into two types by their generation cross sections whose negative midgap gate voltage shifts, ΔV_{MG}, versus electron fluence are shown in Figure 5.2. Type 1 is generated at low electron fluence (less than 10^{16} electrons/cm^2)[46,54,60,63,64]. Type 2 is generated at higher electron fluence (~10^{18} electrons/cm^2) and after initial electron trapping (an increase followed by decrease in ΔV_{MG}) [51-53,59,61,62]. Only type 2 has been studied extensively in the literature[51-53,58,59,61,62], shown to be water related[51,61], and related to positively charged fast donor interface state[51]. However, cautions must be taken when interpreting the generation cross-section as a unique signature to distinguish the traps because it is an effective cross-section of several generation, injection, emission, transport, reaction and capture processes in series, rather than the fundamental definition of the positive oxide charge generation rate divided by the hole flux. Evidently, the use of the electron flux or fluence contributes to the wide spread of the generation cross section

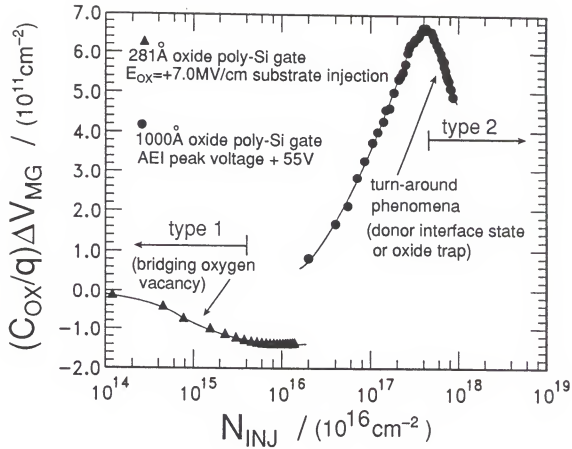

Fig. 5.2: Midgap voltage shift, ΔV_{MG}, versus electron fluence showing the positive charge formation at low (type 1) and high (type 2) electron fluence. The curve labeled by the triangular marker is stressed by substrate electron injection at 7.0MV/cm oxide field. The curve labeled by the circular marker is stressed by avalanche electron injection (AEI) with a peak voltage of 55V from Hsu, Pan and Sah[14].

observed for type 2[51] since if the mechanism is due to hole capture, then the hole flux or hole fluence should be used to compute the cross-section.

In this chapter, we present experimental data on the type 1 positive oxide charge. Six possible mechanisms that may create positive oxide charge are labeled as (1), (2), (3), (4), (5), and (6) in Figure 5.1. They have different electric field, temperature, kinetic energy or accelerating voltage, and electron fluence dependences. To delineate the mechanism responsible for type 1 positive oxide charge, four sets of experiments are performed: (i) the kinetics of positive charge generation and neutralization of the positive traps by electron capture, (ii) the oxide current density, temperature, and gate oxide processing dependences of positive charge generation, (iii) the location of the positive charge through centroid measurements, and (iv) the electron threshold energy for positive charge generation. These suggest that the type 1 positive oxide charge arises from electron impact emission of a trapped electron from an initially neutral oxide trap. Since the impacting electron flux or fluence, measured by the gate current, is used to calculate the cross-section, the experimental impact emission cross-section is a fundamental parameter. Additional experimental evidence supports that the positive oxide charge arises from impact ionizing the bridging oxygen vacancy, $[(Si\text{-}O)_3{\equiv}Si\cdot \cdot Si{\equiv}(O\text{-}Si)_3]$. The bridging oxygen vacancy center in SiO_2 was recognized to be an important intrinsic defect by Sah[69] in 1976 and by R N. Hall in 1966. As discussed recently by Sah and Hsu[14], (i) a higher concentration of the bridging oxygen vacancy is expected in integrated circuit grade oxide exposed to an oxygen deficient ambient and (ii) -1, 0, +1, and +2 charge states of the defect are expected to exist. The

experiments to be presented are consistent with these anticipations. For example, in addition to the observed deep (7eV) +1 charge state in our samples, a shallow (1eV) -1 charge state is also measured after electron capture at oxide traps. These charge states (-1,0,+1) and energy levels (E_C - 1eV) and (E_C - 7eV) are consistent with that of the bridging oxygen vacancy[14]. Furthermore, oxide process dependence studies show that the oxygen deficient oxides have a higher density of shallow oxide traps (-1 charge state) and a higher density of positive oxide charge(+1 charge state), consistent with the bridging oxygen vacancy.

5.2 Experimental Method

5.2-1 Sample Preparation

Polycrystalline silicon-gate bipolar-metal-oxide-semiconductor transistor(BiMOS) test structures[23] were fabricated on an oxidized (100) oriented boron-implanted p-well on a n^-/n^+ substrate. The gate oxide was thermally grown using industrial 850C dry/wet/dry, 900C dry, and 900C dry (0.3% trichloroethane) processes. Gate oxide thicknesses of 86 to 281A were used in this study. Immediately following the gate oxide growth, a 3500A thick polycrystalline silicon film for the gate electrode was deposited and doped n-type by $POCl_3$. The self-aligned source and drain junctions were made by implanting 1.0 x $10^{15}cm^{-2}$ 60KeV phosphorus ions. The implantation damage was annealed at 850C for 30 minutes and subsequent high temperature steps. A drive-in diffusion followed at 900C for 30 minutes in dry nitrogen. The final high temperature processing step was a post-oxidation anneal in either N_2 or O_2 at a high temperature (800-1000C) for 2 hours. High purity VLSI-MOS purity aluminum was then thermally

evaporated and then patterned to form the ohmic contact to the n+ source and drain through their oxide window and to the polycrystalline silicon gate. There was no low-temperature passivation layer. The geometry is reentrant and the gate area is $0.00389cm^2$.

5.2-2 Measurement Setup

Substrate electron injection using the BiMOS structure allows independent control of the oxide electric field and the oxide electron current density[23-12]. Details of the experimental setup and BiMOS test structure were described previously [23,21]. The gate oxide stress condition during an experimental run is determined by the applied oxide voltage (V_{OX}) and the substrate injected electron fluence (N_{INJ}) monitored by the integrated gate current density. The stress is periodically stopped to measure the gate capacitance versus gate voltage (C_G-V_G) and drain current versus gate voltage (I_D-V_G) curves at the stress temperature. Under the stress conditions used in these experiments, parallel gate voltage shifts of the C_G-V_G curves and also I_D-V_G curves were observed which indicated negligible generation of new interface states. The gate voltage shifts of the I_D-V_D and C_G-V_G curves were also identical indicating areally uniform oxide charge generation because the I_D-V_G curve is sensitive to oxide charge located near the source while the C_G-V_G curve is sensitive to oxide charge along the entire surface channel between the source and drain. From the C_G-V_G characteristics, the initial oxide charge density is less that $10^{10}cm^{-2}$ and the initial interface trap density between flatband (V_S=0) and inversion (V_S=2Φ_F) is $10^{10}cm^{-2}$.

5.3 Results

5.3-1 Positive Oxide Charge Generation and Neutralization by Electron Capture

In this section, we show that the positive charged oxide defect is an electron trap and can be neutralized by capturing an electron from the oxide conduction band. The neutralized oxide trap will remain neutral unlike the previously reported positive fast donor Si/SiO_2 interface states (type 2 positive charge) whose charge state will change with the silicon Fermi level or the gate voltage during a measurement of the C_G-V_G curve. Positive oxide charge in these samples were generated during (i) Fowler-Nordheim electron tunneling from the silicon gate or substrate and (ii) BiMOS substrate electron injection at high oxide fields. Regardless of the generation processes, these generated positive charges are completely neutralized by electrons injected into the oxide conduction band from the crystalline silicon substrate at low oxide fields, sufficiently low so that more positive oxide charges are not generated. The measured electron capture cross section is observed to depend only on the oxide electric field and not on the substrate accelerating voltage (collector-base reverse bias voltage). Such an independence on the accelerating voltage or initial kinetic energy of the injected electrons is expected if the positive oxide traps are located farther than several electron scattering lengths from the interface. Centroid measurements in the next section, Section 5.3-4, support this anticipation.

In this section, 5.3-1, we use a two-part stress cycle to measure the oxide field dependence of the electron capture cross section. It consists of (i) tunneling a low electron fluence from the poly-Si gate at high oxide field

(-8.5 to -8.0MV/cm) to generate, create, or form the positive oxide traps, followed by (ii) substrate electron injection at lower field (0.5 to 5.0MV/cm) to neutralize the positive oxide traps.

During low oxide electron fluence (less than $10^{-3}C/cm^2$ or $10^{16}electrons/cm^2$) at high oxide electric fields (greater than 5MV/cm), a negative parallel shift of the C_G-V_G and I_D-V_G curves is observed indicating areally uniform generation of positive oxide traps by the injected electrons. Figures 5.3 and 5.4 show a negative parallel shift of the C_G-V_G and I_D-V_G curves from the original unstressed case, curve-0, after $1.7x10^{15}electron/cm^2$ are tunnel injected into the oxide at E_{OX} = –8.5MV/cm from the gate in the 210A (900C) dry oxide. Subsequent substrate electron injection at low oxide field (1.25MV/cm) results in a positive parallel shift of the curves from curve-1 to curve-2 (after $9.4x10^{13}electron/cm^2$) and to curve-3 (after $8.8x10^{14}electron/cm^2$) which is back to the initial position or curve-0. This confirms the capture of electrons at the positive oxide traps. During the low-field electron capture at the positive oxide traps, negligible oxide charging due to electron capture at existing neutral oxide traps is observed in this fluence range because the electron capture cross section of the neutral oxide traps is several orders of magnitude smaller ($10^{-17}cm^{-2}$ [23]) than that of the positive oxide traps ($\sim 10^{-15}cm^{-2}$). Further electron injection into the oxide at low oxide field produces a small positive parallel shift in the C_G-V_G curve, 0.05V after $1x10^{18}cm^{-2}$ electron fluence which is probably due to electron charging of existing and newly generated neutral electron traps. Generation of interface traps is small during the two-part stress experiment as

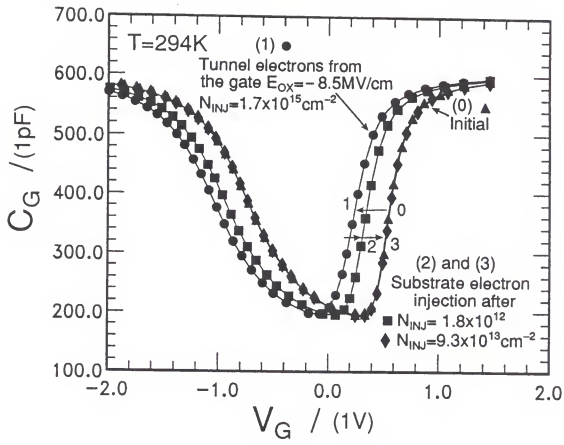

Fig. 5.3: C_G-V_G curves for two-part stress cycle on 210A dry(900C) and 0.3% TCE oxide annealed for 2hr. at 950C: initial curves (triangle), (i) after low fluence at high oxide field positive charge generation (circle) followed by (ii) substrate electron injection at low field (square and diamond). Substrate injection stress conditions: oxide current, J_{OX}=0.03μA/cm, collector base reverse bias accelerating potential, V_{CB}=3.5V, and oxide field, E_{OX}=1.25MV/cm.

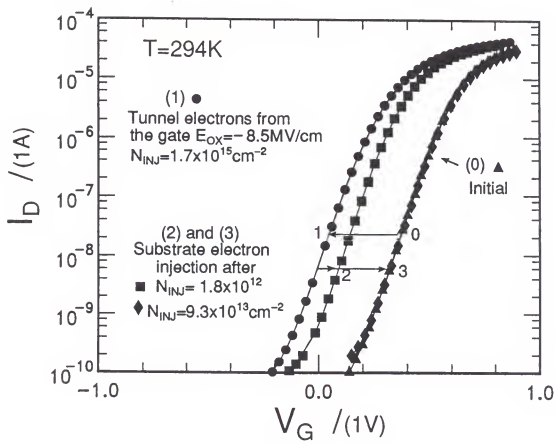

Fig. 5.4: I_D-V_G curves for two-part stress cycle on 210A dry(900C) and 0.3% TCE oxide annealed 2hr. at 950C: initial curves (triangle) (i) after low fluence at high oxide field positive charge generation (circle) followed by (ii) substrate electron injection at low field (square and diamond). Substrate injection stress conditions: oxide current, J_{OX}=0.03μA/cm, collector base reverse bias accelerating potential, V_{CB}=3.5V, and oxide field, E_{OX}=1.25MV/cm.

demonstrated by the very small distortion in the C_G-V_G curve. This two-part stress cycle has been repeated 5 times on the same device and is found to be completely reversible with negligible distortion in the C_G-V_G curve. Figure 5.5 shows the shift in the C_G-V_G curve from repeating the the two-part stress experiment on the device previously stressed in Figure 5.3. Figures 5.5 and 5.3 are essentially identical, demonstrating complete reversibility of charging-discharging or ionization-neutralization of the oxide traps.

The field dependent electron capture cross section at the positive charged oxide trap is measured by repeating the low-field electron injection at several low oxide fields. The positive oxide traps were generated during part one of the stress (-8.0MV/cm oxide field and $2.9 \times 10^{14} cm^{-2}$ tunnel electrons from the gate). Figure 5.6 shows the gate voltage shift of the I_D-V_G curve during the second part (low field electron injection) of the stress cycle versus electron fluence for oxide fields between 0.6 to 1.6MV/cm. This shift is due to the low-field electron capture at the positive oxide trap. The gate voltage is monitored at 1μA drain current and 0.1V drain-to-source voltage. The gate voltage shift is measured from the start of the low-field electron injection. Therefore, it gives the density of electrons captured at the positive oxide traps. These defects were previously ionized positively by a low electron fluence during the high-field stress at -8.0MV/cm. The gate voltage shift versus fluence curves are least-squares fitted to

$$\Delta V_G = A[1 - \exp(-\sigma_n^t N_{INJ})] \qquad (5.1)$$

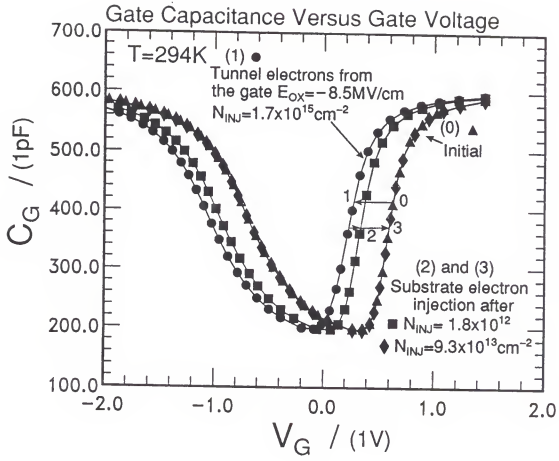

Fig. 5.5: C_G-V_G curve for the same two step stress cycle repeated on the same device in Figure 5.3, indicating complete reversibility (coincidence of curves 0 and 3) and negligible new trap generation.

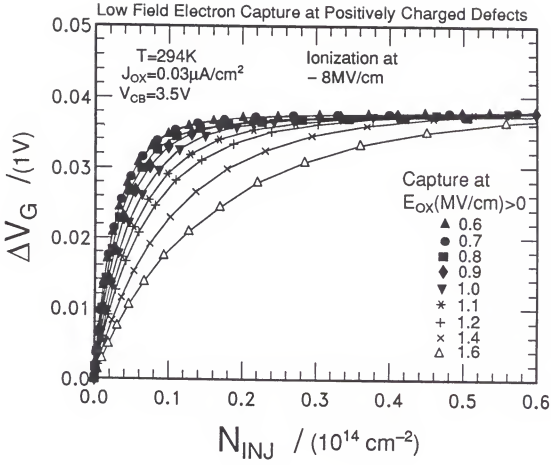

Fig. 5.6: Gate voltage shift versus electron fluence due to electron capture at positively charged defects generated in 2 hr. 950C N_2 annealed 210A dry(900C) and 0.3% TCE oxide. The positively charged defects are generated by tunneling electrons from the gate at -8.0MV/cm for 10sec to a 2.9×10^{14}cm^{-2} electron fluence. Next, the gate voltage versus substrate electron injection is measured at oxide field between 0.5 to 1.6MV/cm.

where σ_n^t is the thermal electron capture cross section. The least-squares-fit equations are plotted as the solid lines in Figure 5.7. The root-mean-square error in the capture cross section is less than four percent as indicated in the table in Figure 5.7. Figure 5.8 gives the oxide electric field dependence of σ_n^t. It shows a strong dependence above 0.6MV/cm, proportional to E_{OX}^{-n} where n ranges from 2 to 4 for oxide fields between 0.6 to 7.0MV/cm. Ning observed a similar E_{OX} dependence for a fabrication-process induced positive electron trap in the oxide field range of 0.5 to 3.0MV/cm[70].

5.3-2 Oxide Current Density Dependence of Positive Oxide Charge Creation

In this section, we show that the positive oxide charge creation rate is proportional to J_{OX} but its steady-state density is independent of J_{OX}. The positive charge creation rate is observed to approach zero, $dn^+_{OT}/dt=0$, after the electron fluence exceeds about $(\sigma_n^t)^{-1}$. This is due to the steady-state balance between the neutralization of positive traps by electron capture and ionization of the neutralized traps by the proposed impact ionization mechanism. This steady-state suggests that the neutralization and ionization rates are proportional to the oxide electron current density. The positive charge creation rate via trap-to-band impact emission [transition (3) in Figure 5.1], band-to-band impact generation [transition (5)], and hole injection from the anode [transition (4)] are all proportional to the oxide current density, J_{OX}, while trap-to-band tunneling emissions, [transitions (1) and (2)], are independent of J_{OX}.

Figures 5.9 and 5.10 plot $\Delta V_G C_{OX}/q$ versus time and electron fluence, respectively, for two values of oxide current density obtained on previously

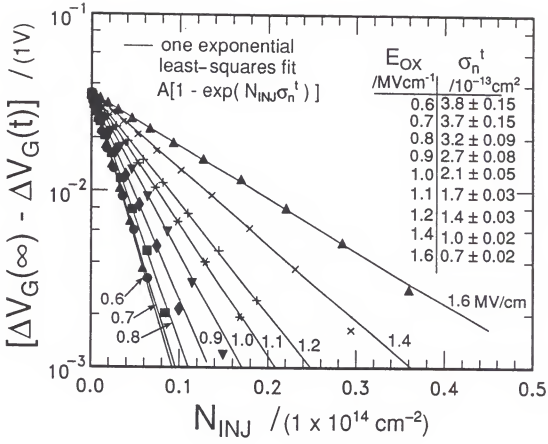

Fig. 5.7: One-exponential least-squares-fit (LSF), $A[1-\exp(N_{INJ}\sigma_n^t)]$, to data in Figure 5.6.

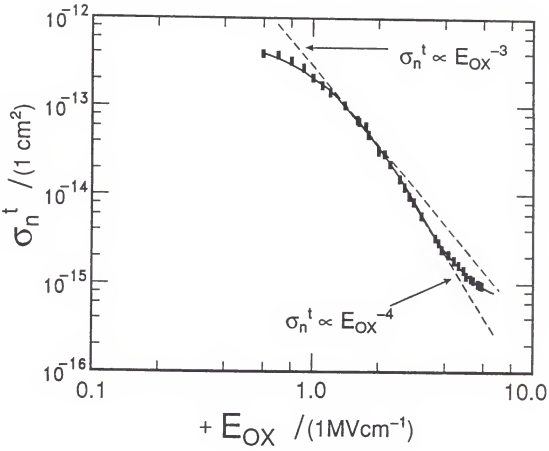

Fig. 5.8: Electron capture cross section from LSF in Fig. 5.7 versus oxide field.

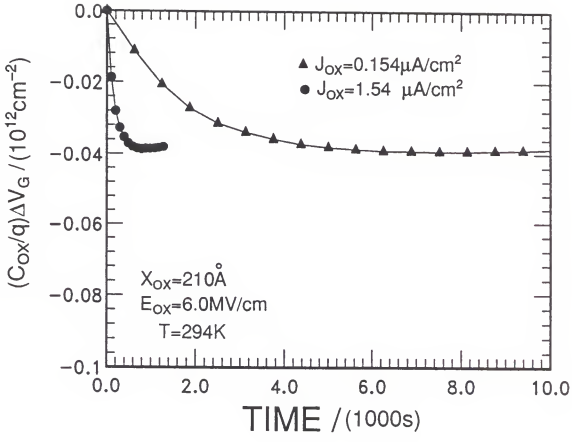

Fig. 5.9: Gate voltage shift due to electron generated positive oxide charge versus stress time at oxide current density, J_{OX}, between 0 to 1.54μA/cm^2. [210A dry(900C) and 0.3% TCE oxide and 2 hr. 950C N_2 anneal].

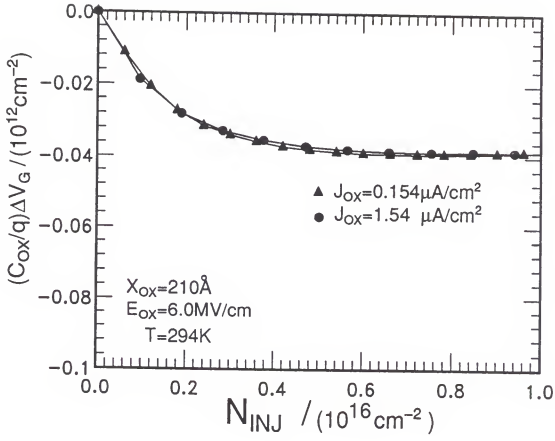

Fig. 5.10: Gate voltage shift due versus electron fluence at oxide current density, J_{OX}, between 0 to 1.54μA/cm^2. [210A dry(900C) and 0.3% TCE oxide and 2 hr. 950C N_2 anneal).

unstressed samples. The gate voltage shift is related to the density of positive oxide traps by

$$\Delta n_{OT}^{+} = - (X_{OX}/X_{OT}) (C_{OX}/q) \Delta V_G \qquad (5.2)$$

where X_{OT} is the centroid for the positive oxide traps measured from the gate, X_{OX} the oxide thickness, and C_{OX} is the oxide capacitance. Figure 5.9 shows that the positive charge generation rate is higher at the higher oxide current density which is consistent with hole injection from the anode, (4) followed by (9) in Fig. 5.1; trap-to-band impact emission, (3); and band-to-band impact generation, (5) followed by (11); but is inconsistent with the trap-to-band tunneling emission mechanism, (1) and (2). The gate voltage shift versus fluence in Fig. 5.10 is observed to be independent on the oxide current density.

In Fig. 5.10, the positive charge creation rate approaches zero, $dn^{+}_{OT}/dt=0$, after about $10^{16}cm^{-2}$ electron fluence independent of the oxide current density. This is attributed to the identical (proportional) gate-current-density (J_{OX}) dependence of the neutralization rate of positive traps by electron capture and ionization rate of the neutralized traps by the proposed generation mechanism.

The kinetic equation governing positive charge formation due to trap-to-band electron impact emission is

$$dn_{OT}^{+}(t)/dt = (J_{OX}/q) [(e_n^n/\Theta_n) n_{OT}(t) - \sigma_n^{+} n_{OT}^{+}(t)] \qquad (5.3)$$

where $n_{OT}^{+}(t)(cm^{-2})$ is the areal density of positive oxide traps as measured by the gate voltage shift, $e_n^n(cm^3/s)$ is the electron impact emission coefficient of trapped electrons, $n_{OT}(t)(cm^{-2})$ is the density of trapped electrons or neutral oxide traps, and $J_{OX}(A/cm^2)$ is the oxide current. The electron thermal and scatter-limited drift velocities are assumed equal and constant, denoted by Θ_n. The total trap density, N_{OT}, is equal to

$$N_{OT} = n_{OT}(t) + n_{OT}^{+}(t) \tag{5.4}$$

and is assumed constant although prolonged experiments at high fields may create new oxide traps which increase N_{OT}. Experiments in Section 3.3-5 show that $N_{OT} >> n_{OT}^{+}$ so $n_{OT} = N_{OT}$. In Eq. (5.3), note that the ionization rate or reciprocal time constant due to impact generation is proportional to the oxide current density, J_{OX}, which is consistent with the data in Figure 5.10. Positive charge formation due to hole injection from the anode and subsequent hole capture, (4) in Figure 5.1, is governed by a similar first order kinetic equation where the coefficient for the ionization term is due to hole capture and the hole density is also proportional to J_{OX}.

The kinetic equation for positive oxide charge resulting from trap-to-band tunneling emission from neutral traps, transitions 1 and 2 in Figure 5.1, is

$$dn_{OT}^{+}(t)/dt = \omega_n n_{OT}(t) - (J_{OX}/q)\sigma_n^t n_{OT}^{+}(t) \tag{5.5}$$

where ω_n is the trap-to-band tunneling emission rate. Thus, (i) the positive charge creation rate, $\omega_n n_{OT}$, is independent of J_{OX}, and (ii) the magnitude

of the saturated gate voltage shift should decrease as J_{OX}^{-1} rather than independent of J_{OX} as indicated by Figure 5.10.

The kinetics of positive charge formation due to hydrogen released from the gate contains hydrogen bond breaking at the gate, hydrogen diffusion in the SiO_2, and the hydrogenation-dehydrogenation reaction at the defects or proton traps. The kinetics proposed for the type 2 positive charge is second order[51,53] rather than the first order observed here. For the band-to-band or interband impact emission, transition 5 in Figure 5.1, the electron threshold energy is greater than the SiO_2 energy gap (~9eV). The threshold energy is measured in Section 3.3-5 and found to be smaller than the SiO_2 energy gap. Thus, these two models will not be considered here since they are inconsistent with our experiments.

Eq. (5.3) describes the impact generation process (or hole injection from the anode with appropriately modified coefficients). Its solution is given by

$$n_{OT}^{+}(t) = N_{OT} \left[1 + \sigma_n^t (\Theta_n / e_n^n) \right]^{-1} (1 - e^{-t/\tau}) \qquad (5.6)$$

where $1/\tau = (J_{OX}/q)(e_n^n/\Theta_n)\left[1 + \sigma_n^t (\Theta_n / e_n^n) \right]$ (5.7)

The steady-state shift is given by

$$\Delta N_{OT}^{+} = n_{OT}^{+}(\infty) = N_{OT} / \left[1 + (\sigma_n^t \Theta_n / e_n^n) \right] \qquad (5.8)$$

The steady-state shift is independent of the oxide current density which is consistent with the measured data in Figures 5.9 and 5.10.

Equations (5.7) and (5.8) give the following general results on the time constant, τ.

$$\Delta N_{OT}^{+} \cdot \tau^{-1} = (J_{OX}/q)\,(e_n^n/\Theta_n)\,N_{OT} = dn^{+}_{OT}(t=0)/dt \qquad (5.9)$$

and

$$J_{OX}\sigma_n^t / q = (1 - \Delta N_{OT}^{+} / N_{OT}) \cdot \tau^{-1}. \qquad (5.10)$$

If $e_n^n << \sigma_n^t \Theta_n$, which is valid at low and moderate electric field, then (9) shows $\Delta N_{OT}^{+} << N_{OT}$ and (10) becomes

$$\tau^{-1} = \frac{J_{OX}(\sigma_n^t/q)}{(1 - \Delta N_{OT}^{+}/N_{OT})}$$

$$= J_{OX}\sigma_n^t/q \ . \qquad (5.11)$$

Thus, the time constant will give the capture cross-section of the positive oxide trap. In the next section, σ_n^t is measured versus E_{OX} from the time constant derived from the initial slope, (9), using the measured ΔN_{OT}^{+}. It is found to be in excellent agreement with the electron capture cross-section by the positive traps shown in Figure 5.8. This consistency provides further confidence in the proposed impact emission model.

5.3-3 Temperature Dependence of Positive Oxide Charge Formation

The temperature dependence of the positive charge creation rate can be used to determine if the creation mechanism is thermally activated [transition (6)]. The creation of the type 2 positive charge was previously reported to be strongly dependent on temperature and suppressed at higher temperatures[61]. Figures 5.11 and 5.12 plot $\Delta V_G C_{OX}/q$ versus electron fluence at 294K and 77K and oxide fields between 4-7MV/cm. The positive

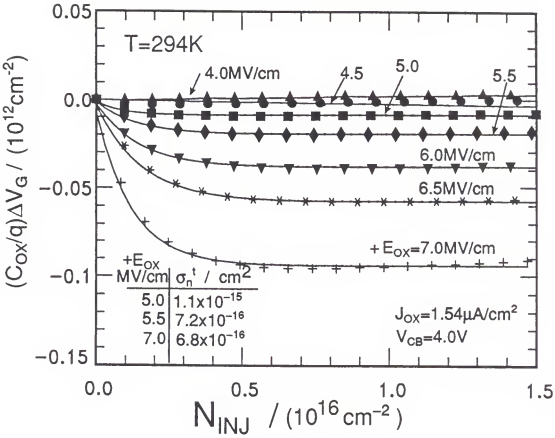

Fig. 5.11: Gate voltage shift due to electron generated positive oxide charge versus electron fluence at oxide fields between 4 to 7MV/cm and T=294K. (2 hr. 950C N_2 anneal 210A dry(900C) and 0.3% TCE oxide).

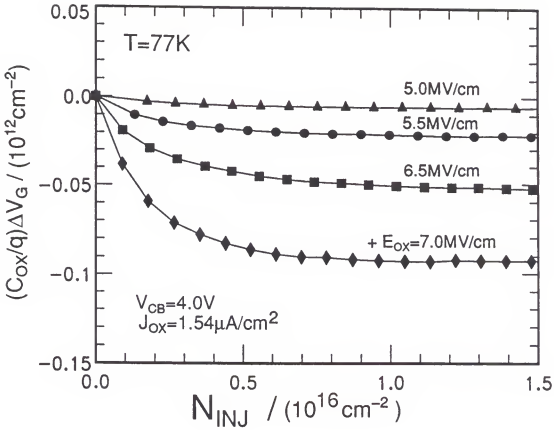

Fig. 5.12: Gate voltage shift due to electron generated positive oxide charge versus electron fluence at oxide fields between 4 to 7MV/cm and T=77K. (2 hr. 950C N_2 anneal 210A dry(900C) and 0.3% TCE oxide).

charge generation is identical at 77 and 294K. Therefore, the generation process for this type 1 positive charge is not thermally activated in the temperature range from 77 to 294K in contrast to the previously reported large temperature dependence of type 2.

The data in Figure 5.11 are least-squares fitted to the one exponential given in Eq. (5.6) to obtain τ. The capture cross section is obtained from the time constant using Eq. (5.11). The values for σ_n^t shown in Figure 5.11 are nearly identical to the values measured independently in Figure 5.8. The agreement of σ_n^t obtained in the electron capture or positive oxide charge neutralization measurements (Figure 5.8) and positive oxide charge generation measurements (Figure 5.11) indicates that neutralization of positive oxide traps by electron capture limits the buildup of net positive charge to a steady-state value after an electron fluence of approximately $(\sigma_n^t)^{-1}$.

The least-squares-fit values of the pre-exponential factor obtained from fitting the data in Figs. 5.11 and 5.12 to Eq. (5.6) are used to obtain e_n^n at 77 and 294K versus oxide field. The values are shown in Figure 5.13. An impact emission coefficient can also be defined in analogy to the interband case[4],

$$\alpha_n^n = (e_n^n/\Theta_n)\,(N_{OT}/x_{OX}) \qquad (5.12)$$

From the values of e_n^n in Figure 5.13, α_n^n is calculated and shown in Figure 5.13. This gives α^n=3500cm^{-1}exp(-33/E_{OX}) where E_{OX}(MV/cm). N_{OT} is taken to be 10^{12}cm^{-2} (measured in Sec. 3.3-6). Our measured values for

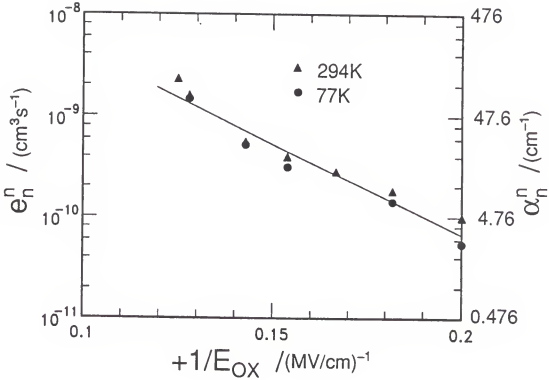

Fig. 5.13: Measured trap-to-band impact emission coefficient obtained from Figure 5.5.

α_n^n, n_{OT}^+ and σ_n^t at 77K are nearly identical to the measured values at 294K, indicating that the type 1 positive charge generation mechanism is not thermally activated.

Weinberg, Fischetti and Nissan-Cohen[46,64] measured a temperature independent (20 to 294K) time constant, τ, for the steady-state SiO_2 induced hole substrate current given by $\tau=q/(J_{OX}\sigma_n^t)$ which agrees with our measured time to reach steady-state for the creation-neutralization of positive oxide charge and our measured values of σ_n^t (Figs. 5.8 and 11). Both positive charge creation-neutralization and the hole substrate current are observed to reach a steady-state plateau value after an electron fluence of approximately $N_{INJ}=1/\sigma_n^t$ independent of the oxide current density. A steady-state plateau was observed after $N_{INJ} \geq (\sigma_n^t)^{-1}$ independent of the oxide current density between $15nA/cm^2$ to $150\mu A/cm^2$ in this work. Weinberg measured the electron fluence needed to reach a steady-state hole substrate current and found no dependence on the fluence for gate current densities between $1mA/cm^2$ to $1A/cm^2$.

Since the hole substrate current and positive oxide charge are observed to have the same time and fluence dependence over 10 orders of magnitude of oxide current density, and the same temperature independence, they are most likely related to the same mechanism, i.e. electron impact emission proposed here (see below). Weinberg[64] noted that the temperature independent substrate current observed at 20K was inconsistent with the data by Hughes[68] on hole transport in SiO_2. Therefore, the SiO_2 substrate current at 20K cannot be due to band-to-band impact generation or hole injection from the anode. The data in Figure 5.12 alone cannot rule

out hole transport since at 77K and high oxide fields, the hole transit time from the gate to the SiO_2 interface in thin oxides is relatively short (≈ 1ms) [68]. One model to explain both the SiO_2 induced substrate current and positive oxide charge is the proposed trap-to-band electron impact emission. Impact emission creates positive traps in the SiO_2 bulk and near the SiO_2/Si interface. The hole substrate current could result from silicon valance electrons tunneling to positive traps near the interface.

5.3-4 Centroid for the Positive Oxide Traps

To measure the centroid for the positive oxide traps, the technique used by Nissan-Cohen, Shappir and Frohman-Bentchkowsky is employed[60] which monitors the shifts in the gate voltage under negative (V_G^-) and positive (V_G^+) stress at constant Fowler-Nordheim tunneling gate current, I_G, and the shift in the flatband voltage (V_{FB}). The centroid measured from the poly-Si gate/SiO_2 interface is obtained from

$$x_{OT} = x_{OX}\ \Delta v_G^+ / (\Delta v_G^+ + \Delta v_G^-) \qquad (5.13)$$

This technique is similar to the positive and negative photo I-V technique[71,72] since it measures the change in the electric field at both interfaces due to the trapped oxide charge. The technique has several limitations[72]: (i) the electron fluence during the measurement may perturb the oxide charge and (ii) the trapped charge located within the tunneling barrier does not produce a shift in V_G^+ and V_G^- equal to $\Delta V_G^+ = -(qn_{OT}{}^+x_{OT}/\varepsilon_{OX})$.

The first limitation on centroid measurements is not significant if the electron fluence during the I_G-V_G measurement is much less than the electron fluence generating the positive charge. In our experiments the electron fluence during the I_G-V_G measurement was restricted to 10^{-3} times the electron fluence during a stress cycle and had only a small effect on the positive charge generated during substrate electron injection at 6-8MV/cm oxide electric field: less than two percent change in the flatband voltage shift after the measurement of several I_G-V_G curves between stress cycles.

The second limitation occurs because oxide charge (qn_{OT}^+) located within the tunneling barrier does not produce a shift in V_G^+ equal to ($-qn_{OT}^+X_{OT}/\varepsilon_{OX}$). For example, charge located at the gate/SiO_2 and SiO_2/Si interface does not alter the tunneling barrier and hence does not cause a shift in V_G^- and V_G^+, respectively. The second limitation requires the use of ΔV_{FB} rather than ΔV_G^+ in Eq. (5.13) to determine the centroid when charge is located within the tunneling barrier of the SiO_2/Si interface. When charge is located within the tunneling distance of the poly-Si gate/SiO_2 interface, Eq. (5.13) is not valid.

Figures 5.14 and 5.15 plot ΔV_G^-, ΔV_G^+, and ΔV_{FB} versus fluence during (i) substrate electron injection at 7.0MV/cm oxide field and (ii) Fowler-Nordheim electron tunneling from the gate at -8.0MV/cm oxide field. The positive and negative gate voltage shifts are defined at 2.5nA/cm^2 gate current density. Consistent with the data by Nissan-Cohen and co-workers, approximately the same magnitude shift in ΔV_{FB} and ΔV_G^+ is observed indicating the positive charge is not located within the tunneling barrier at the SiO_2/Si interface. The finite slope of the ΔV_G^- curve when N_{INJ} >

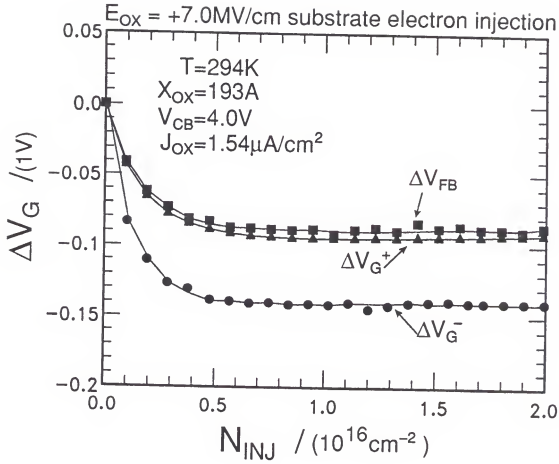

Fig. 5.14: ΔV_G^-, ΔV_G^+, and ΔV_{FB} due to electron generated positive oxide charge during substrate electron injection at E_{OX}=7.0MV/cm.

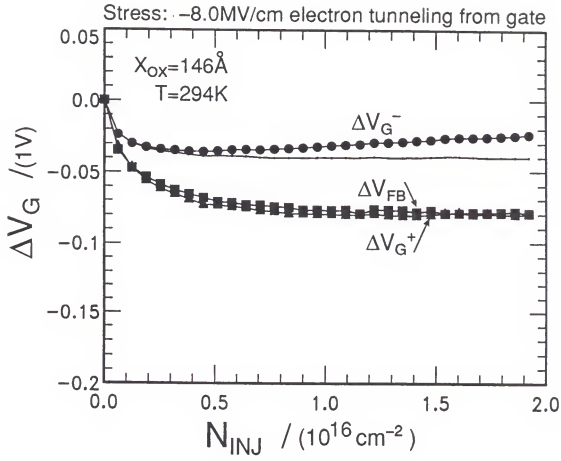

Fig. 5.15: ΔV_G^-, ΔV_G^+, and ΔV_{FB} -8.0MV/cm Fowler-Nordheim tunneling injection from the gate.

$1x10^{16}cm^{-2}$ in Figure 5.15 is indicative of the generation of neutral electron traps which are subsequently charged by capturing an electron[58,23,73]. The oxide electric field dependent neutral trap generation is difficult to minimize during electron injection from the gate (as compared to injection from the substrate) since the electron current density cannot be controlled independently from the oxide field. The electron injection from the gate is at a higher oxide field than injection from the substrate. Approximately 20% of ΔV_G^- at $N_{INJ}=10^{16}cm^{-2}$ is due to the charging of newly generated neutral traps. In determining the centroid for the positive oxide traps versus fluence during tunneling from the gate, the linear generation term is subtracted from ΔV_G^- which gives the thin solid line in Fig. 5.15. Figure 5.16 shows the centroid versus fluence due to electron injection from the gate in the 193A oxide (square marker) and electron injection from the substrate in the 146A oxide (* marker). They were obtained from Figures 5.14 and 5.15 using Eq. (5.13). As seen from Fig. 5.16, the centroid is located in the bulk of the oxide film (i) 110A (in the 193A oxide) from the SiO_2/Si interface during substrate electron injection and (ii) 50A (in the 146A oxide) from the SiO_2/Si interface during gate electron tunneling injection. Figure 5.16 also shows the centroid of the positive charge generated during substrate electron injection at 7.0MV/cm oxide field in 146-281A oxides. For these oxide thicknesses, the measured centroid is 90 to 150A from the SiO_2 interface. Figure 5.17 plots the centroid in the 193A oxide versus substrate injected electron fluence at oxide electric fields between 6-8MV/cm. The centroid for the positive charge is observed to be in the bulk oxide film and moves closer to the cathode (SiO_2/Si interface) at

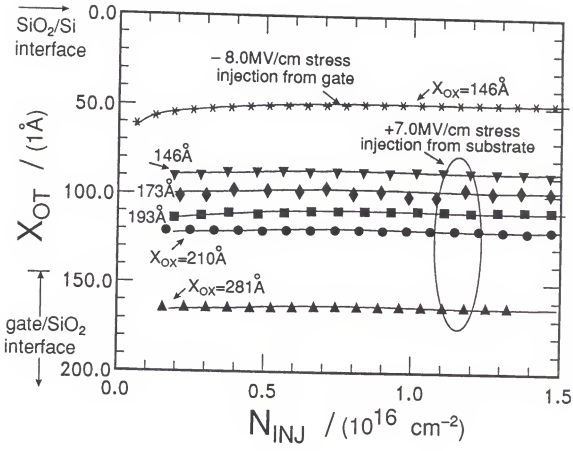

Fig. 5.16: Measured centroid for electron generated positive oxide charge in 146 to 281A dry(900C) oxides (2 hr. 950C N_2 anneal).

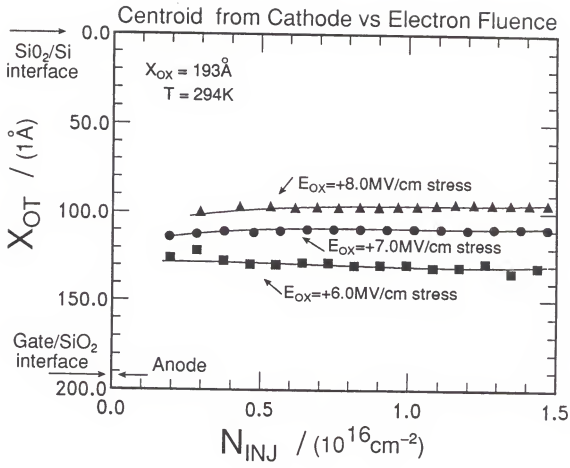

Fig. 5.17: Measured centroid for electron generated positive oxide charge in 193A dry(900C) oxides versus fluence during substrate injection stress at oxide fields between 6 to 8MV/cm (2 hr. 950C N_2 anneal).

higher oxide fields, approaching 90A from the SiO_2/Si interface at E_{OX}=+8.0MV/cm.

It is difficult to account for the centroid data by a model involving hole injection from the anode. Holes have been observed to be relatively mobile in SiO_2 especially at higher temperatures (~294K) and higher oxide field (< 4MV/cm)[68]. The experimental data on hole transport in SiO_2 has been recently reviewed and interpreted by Sah et al.[74]. Previous studies[75,76] on radiation generated holes in SiO_2 indicated a fraction of the holes passing through the oxide are trapped near the SiO_2 interface where the hole trap centroid is expected. For vacuum ultraviolet electron-hole generation near the gate anode, the measured centroid of the trapped holes was oxide field independent and nearer the SiO_2/Si interface[75,76]. For the process of hole injection from the anode during the electron stress at high oxide fields, a similar field independent centroid would be expected. Furthermore, the positive charge in this work is observed to be located outside the tunneling barrier. Only processes in which the hot electron directly creates the positive oxide traps (such as trap-to-band impact emission) preclude the formation of the positive charge near the cathode since electrons within this region have kinetic energy below the impact-emission threshold energy.

The measured trend of the centroid moving towards the anode in thicker oxides and at lower oxide fields is consistent with the threshold kinetic energy that must be gained by the electron in order to impact emit a trapped electron. An energy and spatial distribution of initial neutral traps with a centroid 80 to 90A from the SiO_2/Si interface has been previously

measured by us on these samples[77]. The atomic origin of the traps will be discussed in Section 3.3-6. During electron injection from the substrate, the measured centroid in Figures 5.16 and 5.17 approaches 90A as the oxide thickness decreases from 281 to 146A and approaches 90A as the oxide field increases from 6 to 8MV/cm. This data is consistent with impact emission of trapped electrons from the spatial distribution of initially neutral traps with a centroid 80 to 90A from the SiO_2 interface.

Other researchers[60,78] have observed (i) positively charged defects in the bulk oxide film as opposed to at the gate/SiO_2 and SiO_2/Si interfaces and (ii) the centroid of the positively charged defects moving closer to the cathode with increasing oxide field. Shatzkes and AvRon explained their measured field dependent centroid using the DiStefani and Shatzkes model in which the bulk positive charge comes from immobile band-to-band generated holes[78]. Since the holes in their model are immobile, which they note is inconsistent with experimental data[68], the calculated centroid would be closer to the cathode at higher oxide field because the electrons need to travel a smaller distance from the cathode to reach the threshold kinetic energy for band-to-band impact emission. Their centroid data can also be explained by impact ionization of a defect. The interband impact model requires a large threshold energy [$> E_G(SiO_2)$ ~ 9eV], while the impact detrapping model has a smaller threshold energy, [$< E_G(SiO_2)$]. The latter agrees with data in the following section.

5.3-5 Threshold Voltage for Positive Charge Generation

The approximate threshold voltage for the electron generated positive charge can be obtained from the oxide thickness dependence of the positive

charge generation. Previously, electron generated positive oxide charge was observed to be suppressed in thin oxides (~60A)[48]. Figure 5.18 plots the normalized gate voltage shift versus electron fluence in 86 to 281A oxides stressed at 7.0MV/cm oxide field. Figure 5.19 plots the normalized steady-state gate voltage shift after N_{INJ}=1.0x10^{16}cm^{-2} versus the oxide voltage drop for the 86-281A oxides stressed in Figure 5.18. The steady-state density of electron generated positive oxide traps is observed to increase with increasing oxide thickness. In Figure 5.19, a 7V threshold for the positive charge generation is observed which is similar to the 7-8V threshold observed by Fischetti[48]. However, the positively charged defects observed by Fischetti are likely due to a different atomic defect and generation mechanism since (i) the measurements by Fischetti were on metal gate samples, (ii) the positively charged defects were not observed to capture electrons since no saturation is observed in the positive charge buildup which would be expected due to a steady state balance between electron capture and emission, (iii) the positive charge is located at the SiO_2/Si interface and is accompanied by a large build up of interface states (1x10^{13}cm^{-2}eV^{-1} in the 484A sample), and (iv) the positive charge is observed after initial electron trapping. Therefore, we classify the positive charge observed by Fischetti as type 2 shown in Figure 5.2.

5.3-6 Gate Oxide Processing Conditions

If the positive charge is due to impact emission, there must be a high concentration of initially neutral oxide traps. In this section using gate oxide processing variations, we show that the bridging oxygen vacancy, [(Si-O)$_3$≡Si· ·Si≡(O-Si)$_3$], is the most likely candidate. O'Reilly and

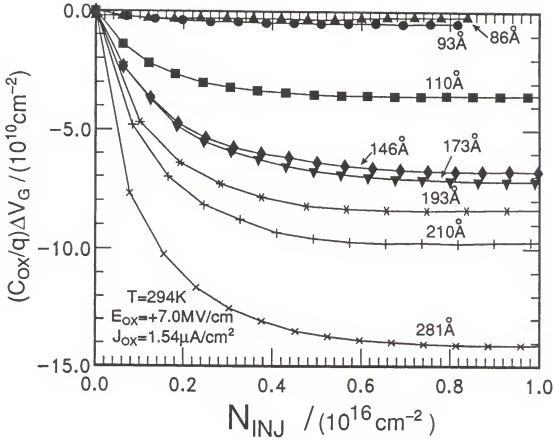

Fig. 5.18: Gate voltage shift due to electron generated positive oxide charge versus electron fluence at 7.0MV/cm oxide fields in 86 to 281A oxides. (2 hr. 950C N_2 anneal).

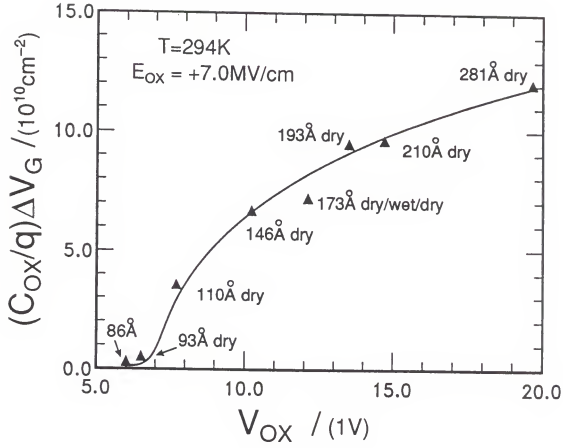

Fig. 5.19: Normalized steady-state gate voltage shift due to the balance between generation-annihilation after N_{INJ}=1.0x10^{16}cm^{-2} versus the oxide voltage drop for 86-281Å oxides stress at 7.0MV/cm oxide field (2 hr. 950C N_2 anneal).

Robertson[16] predicted that the neutral oxygen vacancy has a 7.8eV bound state below the oxide conduction band. This is consistent with the 7.0eV electron threshold energy measured in the previous section. Rudra and Fowler[13] predicted a shallow bound state for the oxygen vacancy with a 0.7eV ± 0.5eV thermal activation energy which is consistent with the shallow electron trap (1eV) observed previously by us[12,77]. In this section, we show that this shallow oxide electron trap is also present in these samples and we find an increased positive charge generation rate (from the deeper 7eV oxide traps) in samples with a higher density of the shallow 1eV traps. Oxide process dependence studies show that oxygen deficient oxides have a larger shallow oxide trap density and positive charge generation rate, pointing to the bridging oxygen vacancy or E′ center.

5.3-6a Process Dependence of Shallow Oxide Traps

The density of states(DOS) of the shallow (1eV) electron trap is measured in 281A dry(900C) oxides annealed in N_2 and O_2 at 800C-1000C. The density of states are calculated using the isochronal-EFSE technique[12,77]. The Price-Sah tunnel emission model[22] extended by Chaudhuri, Coon and Karunasiri[35] is used to analyze the experimental emission data. The effective mass is taken equal to the free electron mass($m^*=m_0$) and the parameter n=0 is used for the neutral potential well that traps the electron. The isochronal EFSE technique, error analysis, and the sensitivity of the results to model parameters have previously been analyzed[77].

Figures 5.20 and 5.21 show the density of states of charged oxide traps in 281A dry(900C) oxides annealed in O_2 and N_2 at 800, 900, and 1000C for

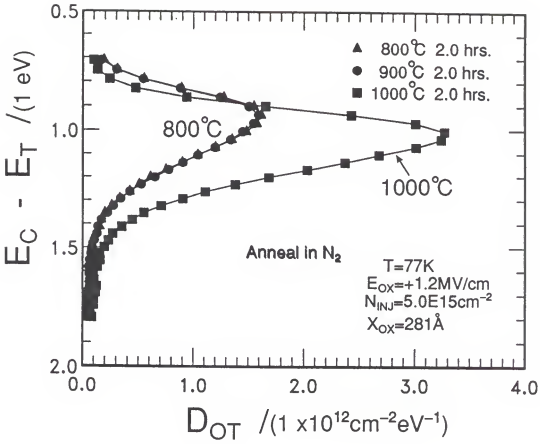

Fig. 5.20: Measured density of state of shallow oxide traps charged at E_{OX}=1.2MV/cm, N_{INJ}=0.5x10^{16}cm^{-2}, and T=77K in 2 hr. 800-1000C N_2 annealed 281A dry(900C) oxide.

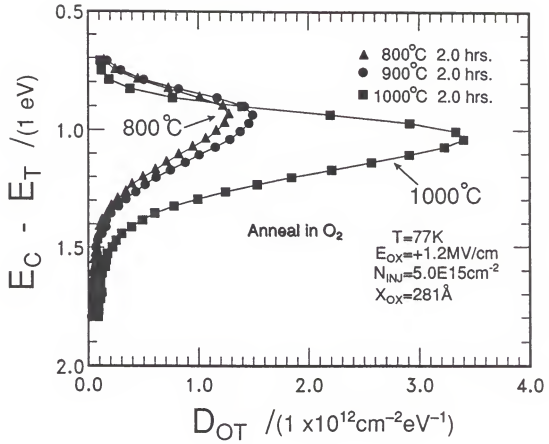

Fig. 5.21: Measured density of state of shallow oxide traps charged at E_{OX}=1.2MV/cm, N_{INJ}=0.5x10^{16}cm^{-2}, and T=77K in 2 hr. 800-1000C O_2 annealed 281A dry(900C) oxide.

two hours. An 0.5 x $10^{16}cm^{-2}$ electron fluence was used to charge the oxide traps at 77K. To calculate the density of states, a centroid equal to the oxide thickness is used. The peak in the density of states is about 1eV for all the samples. There is a slight shift in the density of states peak for the 1000C annealed sample from 1.0 to 1.2eV. The shift in the DOS peak is due to the trapped electrons altering the local oxide field at the trap[77]. At lower electron fluence and trapped charge, the peak in the DOS for the 1000C annealed samples is 0.95eV. The 800 and 900C O_2 and N_2 annealed samples have approximately the same oxide trap density. A significantly higher density of shallow oxide traps is observed in both the 1000C N_2 and O_2 annealed samples. The data in Figures 5.20 and 5.21 are suggestive of the oxide electron trap originating from an oxygen vacancy since N_2 anneals at 800-1000C create an oxygen deficient ambient and increases oxygen vacancy density. The O_2 anneal of a polycrystalline-Si/oxide/Si system should also create an oxygen deficient oxide since the oxide is sandwiched or located between a polycrystalline-Si and crystalline Si layers which effectively block the diffusion of oxygen into the oxide.

The N_2 and O_2 annealing studies by Balk, Aslam, and Young[30] are indeed consistent with our bridging oxygen vacancy model, $[(Si\text{-}O)_3{\equiv}Si\cdot \cdot Si{\equiv}(O\text{-}Si)_3]$, or a trivalent silicon or silicon dangling bond, $[(Si\text{-}O)_3{\equiv}Si\cdot]$. They found that a N_2 anneal above 900C increased the defect density and an O_2 anneal prior to polycrystalline-Si gate deposition decreased the defect density. The trivalent silicon defect can explain the annealing data but the negatively charged state is expected to have an 2.0eV[44] electron binding energy which is deeper than our measured 0.9eV. Therefore, we prefer the

bridging oxygen vacancy model to explain the initially neutral oxide defect in both our and their samples.

5.3-6b Process Dependence of Positive Charge Generation

Figures 5.22 and 5.23 show the gate voltage shift from positive charge generation at high oxide field (4-7MV/cm) versus electron fluence in oxides annealed in 800C N_2 and 1000C N_2. The samples annealed in 800C O_2, 900C N_2 and 900C O_2 have nearly identical characteristics to those annealed in 800C N_2 shown in Figure 5.22. The 1000C O_2 annealed sample has nearly identical characteristics to those annealed in 1000C N_2 shown in Figure 5.23. A significant increase in the electron generated positive charge is observed in the samples with a higher concentration of shallow oxide traps (from higher annealing temperature, such as 1000C) as seen in Figures 5.20 and 5.21. This is consistent with the larger positive charge generation during Fowler-Nordheim tunneling stress of polycrystalline-Si gate capacitors annealed at temperatures above 900C observed by Holland and Hu[79]. A correlation between the $[(Si\text{-}O)_3{\equiv}Si\cdot \cdot Si{\equiv}(O\text{-}Si)_3]$ defect and the electron generated positive charge is expected for the two generation mechanisms: (i) trap-to-band impact emission at the oxygen vacancy and (ii) hole trapping since the bridging oxygen vacancy is also a hole trap[3].

During positive charge (type 1) generation experiments on these samples, electron capture at initially neutral traps does not significantly alter the local oxide field to enhance positive charge generation in contrast to positive charge generation measurements on samples with a large concentration of water related or intentionally introduced electron traps (type 2)[51,62]. In our samples, the density of water related electron traps,

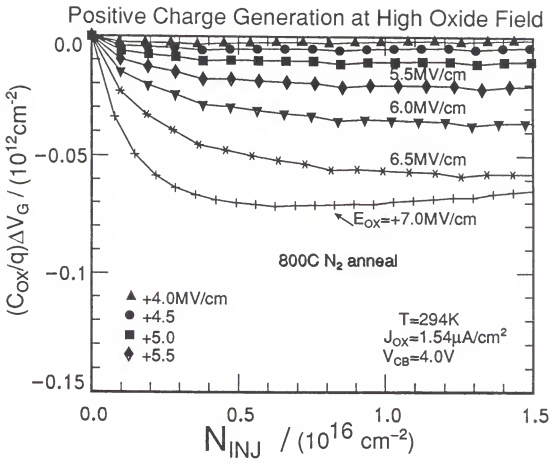

Fig. 5.22: Gate voltage shift due to electron generated positive oxide charge versus electron fluence at oxide fields between 4 to 7MV/cm. [2 hr. 800C N_2 annealed 281A dry(900C) oxide].

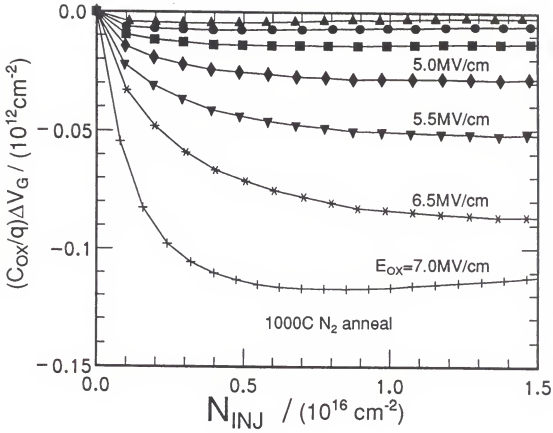

Fig. 5.23: Gate voltage shift due to electron generated positive oxide charge versus electron fluence at oxide fields between 4 to 7MV/cm. [2hr. 1000C N_2 annealed 281A dry(900C) oxide].

measured by charging at low oxide field and room temperature, is small and approximately the same in all the 800-1000C O_2 and N_2 annealed samples as measured from the gate voltage shift at large electron fluence($10^{18}cm^{-2}$). The gate voltage shift in the 281A oxide after $10^{18}cm^{-2}$ electron fluence at oxide fields between 1 to 3MV/cm is less than 0.05V (room temperature negatively charged trap density ~ $5x10^{10}cm^{-2}$). The low concentration of water related traps in these samples facilitates the study of electron generated positive charge since the contribution to the gate voltage shift due to electron capture at the existing water-related neutral traps is small and does not need to be separated from the total gate voltage shift. The trapped negative charge in Al-gate samples is typically much larger than the positive oxide charge and must be subtracted from the data to give the smaller positive oxide charge[48]. The low concentration of existing deep electron traps in the polycrystalline-Si gate oxide used in this and previous studies by Sah, Sun, and Tzou is most likely due to the reduction of the water related traps during the high temperature anneal carefully demonstrated by Sah, Sun and Tzou[53].

5.4 Conclusion

The bridging oxygen vacancy, $[(Si\text{-}O)_3{\equiv}Si\cdot \quad \cdot Si{\equiv}(O\text{-}Si)_3]$ denoted by V_O and E′ -center, was recognized in 1976 by Sah[69] and earlier (1966) by R.N. Hall as a possible donor center in SiO_2 based on a simple bond model. In this chapter, the first donor state, V_O^+, is experimentally demonstrated in state-of-art-oxides for submicron VLSI. Emission of a trapped electron by electron impact at the bridging oxygen vacancy is shown to be a consistent model to account for the positive oxide charge (V^+_O) observed after low

injected electron fluence at high oxide fields (5 to 8.5MV/cm) in 110-281A oxides. It is shown that the positive charge generation and neutralization via electron capture at this oxygen vacancy reaches a steady-state after an electron fluence of 10^{15}-10^{16}cm^{-2} [-$(\sigma_n^t)^{-1}$] for oxide fields between 4-7MV/cm. Above this fluence, no additional net positive oxide charge is formed. A threshold energy of 7eV is measured for impact emission which is consistent with the theoretical calculated bound state energy by O'Reilly and Robertson[16] of 7.8eV for the bridging oxygen vacancy. A shallow electron trapping level located 1eV below the oxide conduction band is measured on the same sample which is consistent with the 0.7 ± 0.5eV (–/0) shallow state of the bridging oxygen vacancy calculated by Rudra and Fowler[13]. The trap density and generation rate increase in oxides annealed in N_2 at 800 to 1000C which is consistent with the oxygen vacancy origin. Experimental measurements indicated that (i) the centroid for the positive charge is in the bulk of the oxide film and its location depends on the oxide stress field and thickness but asymptotically approaching 90A from the SiO_2/Si interface and (ii) the positive charge is not present near the cathode where the electron has not gained significant kinetic energy from the oxide field in order to initiate impact emission. Our observed first order kinetics, temperature independent generation rate from 77-294K, and location of the positive charge in the bulk of the oxide film, all suggest that the positive charge generated at low fluence (type 1) is different than the water-related positive charge or donor interface state (type 2) reported at much higher fluence by previous researchers.

CHAPTER 6
CONCLUSION

Silicon dioxide has and will continue to be an important material in very-large-scale-integrated (VLSI) circuits. The oxide wearout by hot carrier injection in next generation ultra-large-scale-integrated-circuits (ULSI) with 50-100A gate oxides could be more severe due to non-ideal scaling which results in higher oxide and channel electric fields in submicron MOSFETS. To study oxide wearout by hot carrier injection, a substrate injector test structure is used which allows the oxide electric field to be controlled independently from the oxide electron current density. This allows the oxide field dependence of the trap charging-discharging and generation-annihilation processes to be studied.

Industrial 86-281A dry, dry/wet/dry, and partial steam thermal oxides are stressed using substrate electron injection. New experimental data is presented which shows that the oxygen vacancy defect, $[(Si\text{-}O)_3{\equiv}Si\cdot\ \cdot Si{\equiv}(O\text{-}Si)_3]$, is important to gate oxide charging. Two electron bound states for the defect are experimentally measured, a shallow and deep level located 1.0 and 7eV from the oxide conduction band. The shallow state is measured using a new experimental technique which uses trap-to-band tunneling emission of electrons. An energy distribution of shallow oxide traps is found with a density of states at about 1eV. The same density of state versus

trap energy for the oxygen vacancy defect is found in the thermally grown oxide thicker than 150A. A decrease in the density of charged oxide traps is found for oxides less than 100A due to trap-to-gate tunneling emission as predicted by Sah[3,28].

The deep level is concluded from electron generated positive oxide charge experiments. Experimental evidence supports that the positive charge in the bulk oxide film comes from emission of a deep trapped electron by electron impact at an initial neutral oxygen vacancy defect. An electron impact threshold energy of 7eV is measured which is consistent with the theoretical calculated bound state energy of 7.8eV for an oxygen vacancy which relaxes to form a silicon-silicon bond. The oxide thickness dependence (86-281A) of positive charge generation during electron transport is SiO_2 at high electric fields is measured. Significantly less positive oxide charge is generated in oxides with thickness less than 100A. This is attributed to the smaller density of electron in thinner oxides which have the 7.0eV of kinetic energy necessary for electron impact emission.

REFERENCES

[1] D. Kahng and M.M. Atalla, "Silicon-silicon dioxide field induced surface devices," presented at the IRE-AIEE Solid-State Device Research Conference at Carnegie Institute of Technology, Pittsburgh, PA, 1960.

[2] C.T. Sah, "Evolution of the MOS transistor–from conception to VLSI," Proc. IEEE, **76**, 1280 (1988).

[3] C.T. Sah, "Models and experiments on degradation of oxidized silicon," Solid State Electron. **33**, 147 (1990).

[4] C.T. Sah, Fundamentals of Solid-State Electronics (World Scientific Publishing Co., Singapore, 1991), p674.

[5] C.T. Sah, in Properties of Silicon (INSPEC, London, 1988), Ch. 17, p497.

[6] R.N. Switzer, A Computer-Automated Temperature Control System for Semiconductor Measurements, M.S. Thesis, University of Illinois, August 1979.

[7] For a review of these two methods, see: J.P. Fillard and J. van Turnhout, Thermally Stimulated Processes in Solids: New Prospects (Elsevier Scientific Publishing Company, New York, 1977).

[8] C.T. Sah, W.W. Chan, H.S. Fu, and J.W. Walker,"Thermally stimulated capacitance (TSCAP) in p-n Junction," Applied Physics Letters **20**, 193 (1972).

[9] L.D. Yau and C.T. Sah, "Thermal ionization rates and energies of electrons and holes at silver centers in silicon," Physica Status Solidi (a) **6**, 561 (1971).

[10] C.T. Sah, L.L. Rosier and L. Forbes, "Direct observation of the multiplicity of impurity charge states in semiconductors from low-temperature high-frequency photo-capacitance," Applied Physics Letters **15**, 161 and 316 (1969).

[11] C.T. Sah and A.F. Tasch, "Precise determination of the multiphonon and photon carrier generation properties using the impurity photovoltaic effect in semiconductors," Phys. Rev. Letters **19**, 69 (1967).

[12] S.E. Thompson and T. Nishida, "Tunneling and thermal emission of electrons from a distribution of shallow traps in SiO_2," Appl. Phys. Lett. **58**, 1262 (1991).

[13] J. Rudra, W.B. Fowler, "Oxygen vacancy and the E_1' center in crystalline SiO_2," Phys. Rev. B **35**, 8223 (1987).

[14] C.T. Sah and C.C.H. Hsu, in Properties of Silicon (INSPEC, London, 1988), Section 17.5, p532.

[15] D.R. Young, in Proceedings of the Symposium on the Physics and Chemistry of SiO_2 and the Si-SiO_2 Interfac, held at the 173rd Meeting of The Electrochemical Society (Plenum, New York, 1988), p487.

[16] E. P. O'Reilly, J. Robertson, "Theory of defects in vitreous silicon dioxide," Phys. Rev. B **27**, 3780 (1983).

[17] J. Robertson, "Intrinsic defects and hydroxyl groups in a-SiO_2," J. Phys. C **17L**, 221 (1984).

[18] J. Robertson, "Defect mechanisms in a-SiO_2," Philos. Mag. B **52**, 371 (1985).

[19] J. Robertson, in The Physics and Technology of Amorphous SiO_2, R.A.B. Devine, ed. (Plenum, New York, 1988) p91.

[20] N.F. Mott and R.W. Gurney, Electronic Processes in Ionic Crystals (Clarendon, Oxford, 1940), p160.

[21] C.C.H. Hsu, T. Nishida, and C.T. Sah, "Observation of threshold oxide electric field for trap generation in oxide films on silicon," J. Appl. Phys. **63**, 5882 (1988).

[22] C.T. Sah, "Electronic processes and excess currents in gold-doped narrow silicon junctions," Phys. Rev. **123**, 1594 (1961).

[23] T. Nishida and S.E. Thompson, "Oxide field and thickness dependence of trap generation in 9-30nm Dry and Dry/wet/dry oxides," J. Appl Phys. **69**, 3986 (1991).

[24] D.J. DiMaria and J.W. Stasiak, "Trap creation in silicon dioxide produced by hot electrons," J. Appl. Phys. **65**, 2342 (1989).

[25] D.R. Young, E.A. Irene, D.J. DiMaria, R.F. DeKeersmaecker, and H. Z. Massoud, "Electron trapping in SiO_2 at 295 and 77K," J. Appl. Phys. **50**, 6366 (1979).

[26] M. Aslam and P. Balk, in Insulating Films on Semiconductors J. F. Verway and D. R. Wolters, Eds. (Amsterdam, North-Holland, 1983).

[27] A. Ourmazd, D.W. Taylor, J.A. Rentschler, and J. Bevk, Phys. "Si to SiO_2 transformation: interfacial structure and mechanism," Rev. Lett. **59**, 213 (1987).

[28] C.T. Sah, in Proceedings of Technical Papers, 1987 International Symposium on VLSI Technology, Systems, and Applications, Taipei, May 13-15, 1987. (TSPD(C60), ERSO, ITRI; No. 195-4(C60), Chung Hsing Rd., Sec. 4, Chu Tung, Hsinchu, Taiwan (31015), Republic of China), 153 (1987). See especially equation (9).

[29] D.J. DiMaria, "Temperature dependence of trap creation in silicon dioxide," J. App. Phys. **68**, 5234 (1990).

[30] P. Balk, M. Aslam, and D.R. Young, "High temperature annealing behavior of electron traps in thermal SiO_2," Solid-State Electron. **27**, 709 (1984).

[31] M. Aslam, R. Singh, and P. Balk, " Nature of electron and hole traps in MOS Systems with poly-Si electrode," Phys. Status Solidi **84**, 659 (1984).

[32] D.J. DiMaria, "Correlation of trap creation with electron heating in silicon dioxide," Appl, Phys. Lett. **51**, 655 (1987).

[33] R.C. Hughes, "Time-resolved hole transport in a-SiO_2," Phys. Rev. Lett. 35, 449 (1975).

[34] T.H. Ning, "Thermal reemission of trapped electrons in SiO_2," J. Appl. Phys. 49, 5997 (1978).

[35] S. Chaudhuri, D.D. Coon, and R.P.G. Karunasiri, " Impurity-to-band tunneling in semiconductors," J. Appl. Phys. 54, 5476 (1983).

[36] J.R. Banavar, D.D. Coon, and G.E. Derkits, "Low-temperature field ionization of localized impurity levels in semiconductors," Appl. Phys. Lett. 34, 94 (1979).

[37] Z.A. Weinberg, "On tunneling in metal-oxide-silicon structures," J. Appl. Phys. 53, 5052 (1982).

[38] J. Maserjian, in Proceedings of the Symposium held at the 173rd Meeting of The Electrochemical Society (Plenum, New York, 1988), p497.

[39] Z.A. Weinberg and A. Hartstein, "Photon Assisted Tunneling from Aluminum into Silicon Dioxide," Solid State Commun. 20, 179 (1976).

[40] Z.A. Weinberg, "Tunneling of electrons from Si into thermally grown SiO_2," Solid-State Electron. 20, 11 (1977).

[41] R.H. Bube, Photocondutivity of Solids (Wiley, New York 1960).

[42] E.W. Williams, "A photoluminescence study of acceptor centres in gallium arsenide," Brit. J. Appl. Phys. 18, 253 (1967).

[43] F.E. Williams, "An absolute theory of solid-state luminescence,"J. Chem. Phys., 19, 457 (1951).

[44] D.L. Griscom, "Defects structure of glasses," J. Non-Cryst. Solids (Netherlands) 73, 51 (1985).

[45] C.M. Gee and M. Kastner, "Intrinsic-defect photoluminescence in amorphous SiO_2," Phys. Rev. Lett. 42, 1765 (1979).

[46] Z.A. Weinberg, M.V. Fischetti,and Y.Nissan-Cohen, "SiO_2-induced substrate current and its relation to positive charge in field-effect transistors," J. Appl. Phys. **59**, 824 (1986).

[47] N. Klein and P. Solomon, "Current runaway in insulators affected by impact ionization and recombination," J. Appl. Phys. **47**, 4364 (1976).

[48] M.V. Fischetti, Z.A. Weinberg, and J.A. Calise, "The effect of gate metal and SiO_2 thickness on the generation of donor states at the Si-SiO_2 interface," J. Appl. Phys. **57**, 418 (1985).

[49] Z.A. Weinberg and G.W. Rubloff, "Exciton transport in SiO_2 as a possible cause of surface-state generation in MOS structures," Appl. Phys. Lett., **32**, 184 (1978).

[50] Z.A. Weinberg, W.C. Johnson, and M.A. Lampert, "High-field transport in SiO_2 on silicon induced by corona charging of the unmetallized surface," J. Appl. Phys. **47**, 248 (1976).

[51] C.T. Sah, J.Y. Sun, and J.J. Tzou, "Generation-annealing kinetics of the interface donor states at 0.25eV above the midgap and the turn-around phenomena on oxidized silicon during avalanche electron injection," J. Appl. Phys. **54**, 2547 (1983).

[52] C.T. Sah, J.Y. Sun, and J.J. Tzou, "Study of the atomic models of three donor-like traps on oxidized silicon with aluminum gate from their processing dependences," J. Appl. Phys. **54**, 5864 (1983).

[53] C.T. Sah, J.Y. Sun, and J.J. Tzou, "Study of the atomic models of three donorlike defects in silicon metal-oxide-semiconductor structures from their gate material and process dependencies," J. Appl. Phys. **55**, 1525 (1984).

[54] Y. Nissan-Cohen, J. Shappir, and D. Frohman-Bentchkowsky, "Dynamic model of trapping-detrapping in SiO_2," J. Appl. Phys. 58, 2252 (1985).

[55] M.H. Woods and R. Williams, "Hole traps in silicon dioxide," J. Appl. Phys. **47**, 1082 (1976).

[56] Z.A. Weinberg, in The Physics and Technology of Amorphous SiO_2 (Plenum Publishing Corp., New York, 1988), p427.

[57] M.M Heyns and R.F. DeKeersmaecker, "Comparison of high-field stress effects in metal-oxide semiconductor structures with aluminum and polycrystalline silicon gates using internal photoemission measurements," J. Appl. Phys. **58**, 3936 (1985).

[58] D.J. DiMaria and J.W. Stasiak, " Trap creation in silicon dioxide produced by hot electrons," J. Appl. Phys. **65**, 2342 (1989).

[59] C.C.H. Hsu, S.C.S. Pan, and C.T. Sah, "Trap generation during low-fluence avalanche-electron injection in metal-oxide-silicon capacitors," J. Appl. Phys. **63**, 5882 (1988).

[60] Y. Nissan-Cohen, J. Shappir and D. Frohman-Bentchkowsky, "High field current induced-positive charge transients in SiO_2," J. Appl. Phys. **54**, 5793 (1983).

[61] F.J. Feigl, D.R. Young, D.J. DiMaria, S. Lai, and J. Calise, "The effects of water on oxide and interface trapped charge generation in thermal SiO_2 films," J. Appl. Phys. **52**, 5665 (1981).

[62] M.V. Fischetti, "The importance of the anode field in controlling the generation rate of the donor states at the Si-SiO_2 interface," J Appl. Phys. **56**, 575 (1984).

[63] Z.A. Weinberg and T.N. Nguyen, "The relation between positive charge and breakdown in metal-oxide-silicon structures," J. Appl. Phys. **61**, 1947 (1987).

[64] Z.A. Weinberg and M.V. Fischetti, " Investigation of the SiO_2-induced substrate current in silicon field-effect-transistors," J. Appl. Phys. **57**, 443 (1985).

[65] C.M. Osborn and D.W. Ormond, "Dielectric breakdown in silicon dioxide films on silicon," J. Electrochem Soc. **119**, 591 (1972).

[66] T.H. DiStefano and M. Shatzkes, "Impact ionization model for dielectric instability and breakdown," Appl. Phys. Lett. **25**, 685 (1974).

[67] P. Solomon and N. Klein, "Impact ionization in silicon dioxide at fields in the breakdown range," Solid State Commun. **17**, 1397 (1975).

[68] R.C. Hughes, "Time-resolved hole transport in a-SiO_2," Phys. Rev. B **15**, 2012 (1977).

[69] C.T. Sah, IEEE Transactions on Nuclear Science, NS-23, 1563 (1976).

[70] T.H. Ning, "High-field capture of electrons by coulomb-attractive centers in silicon dioxide," J. Appl. Phys. **47**, 3201 (1976).

[71] R.J. Powell and C.N. Berglund, " Photoinjection studies of charge distributions in oxides of MOS structures," J. Appl. Phys. **42**, 4390 (1971).

[72] D.J. DiMaria, "Determination of insulator bulk trapped charge densities and centroids from photocurrent-voltage characteristics of MOS structures," J. Appl. Phys. **47**, 4073 (1976).

[73] M.M. Heyns, R. F. Dekeersmaecker, and M. W. Hillen, "Trap generation and electron detrapping in SiO_2 during high-field stressing of metal-oxide-semiconductor structures," Appl. Phys. Lett. **44**, 202 (1984).

[74] C.T. Sah, A.J. Chen, C.C.H. Hsu, and T. Nishida, in Properties of Silicon, (INSPEC, London 1988), Section 17.18, p613.

[75] R.J. Powell and G. F. Derbenwick, "Vacuum ultraviolet radiation effects in SiO_2," IEEE Trans. Nucl. Sci. NS-18, 99 (1971).

[76] R.J. Powell, "Hole photocurrents and electron tunnel injection induced by trapped holes in SiO_2 films," J. Appl. Phys. **46**, 4557 (1975).

[77] S. E. Thompson and T. Nishida, "A new measurement method for trap properties in insulators and semiconductors: using electric field stimulated trap-to-band tunneling transitions in SiO_2," J. Appl. Phys. **70**, 6864 (1991).

[78] M. Shatzkes, and M. Av-Ron, "Impact ionization and positive charge in thin SiO_2 films," J. Appl. Phys. **47**, 3192 (1976).

[79] S. Holland and C. Hu, "Correlation between breakdown and process-induced positive charge trapping in thin thermal SiO_2," J. Electrochem. Soc. **133**, 1705 (1986).

BIOGRAPHICAL SKETCH

Scott E. Thompson received his B.S. and M.E. in Electrical Engineering from the University of Florida. He received his B.S. degree with highest honors and also won the Outstanding Two Year Scholar of UF and the Outstanding Electrical E Award. He is a member of Tau Beta Pi, Phi Beta Kappa, and Eta Kappa Nu. He completed a thesis masters degree in December 1988 under the supervision of F.A. Lindholm while working as a research assistant in the area of device modeling. He is currently working towards a Ph.D. under the supervision of T. Nishida and C.T. Sah in the area of hot electron reliability of gate insulators in MOS devices. S.E. Thompson has been awarded a Pittman Eminent Scholar Chair Fellowship and an Intel Fellowship.

I certify that I have read this study and that in my opinion it conforms to acceptable standards of scholarly presentation and is fully adequate, in scope and quality, as a dissertation for the degree of Doctor of Philosophy.

K. A. Muttalib
Assistant Professor of Physics

This dissertation was submitted to the Graduate Faculty of the College of Engineering and to the Graduate School and was accepted as partial fulfillment of the requirements for the degree of Doctor of Philosophy.

May 1992

Winfred M. Phillips
Dean, College of Engineering

Madelyn M. Lockhart
Dean, Graduate School